Dynamics of a chemically pulsing mantle plume

Article *in* Earth and Planetary Science Letters · May 2020

DOI: 10.1016/j.epsl.2020.116182

6 authors, including:

Rex Taylor
University of Southampton
180 PUBLICATIONS **10,008** CITATIONS
SEE PROFILE

Pablo Davila-Harris
Instituto Potosino de Investigación Científica y Tecnológica
57 PUBLICATIONS **943** CITATIONS
SEE PROFILE

M. J. Branney
University of Leicester
137 PUBLICATIONS **5,375** CITATIONS
SEE PROFILE

Thomas Gernon
University of Southampton
114 PUBLICATIONS **2,590** CITATIONS
SEE PROFILE

Dynamics of a chemically pulsing mantle plume

Rex N. Taylor[1], Pablo Davila-Harris[2,3], Michael Branney[3], E.M. Ruth Farley[1], Thomas M. Gernon[1], Martin R. Palmer[1].

[1] School of Ocean and Earth Science, University of Southampton, Waterfront Campus, Southampton, SO14 3ZH, UK

[2] Instituto Potosino de Investigación Científica y Tecnológica, San Luis Potosí, Mexico.

[3] Department of Geography, Geology and the Environment, University of Leicester, UK

Upwelling plumes from the deep mantle have an impact on the Earth's surface for tens to hundreds of millions of years. During the lifetime of a mantle plume, periodic fluctuations in its composition and temperature have the potential to generate changes in the nature and volume of surface volcanism. We constrain the spatial and temporal scale of compositional changes in a plume using high-resolution Pb isotopes, which identify chemical pulses emerging from the Canary Islands hotspot over the last ~15 million years (Myr). Surface volcanism spanning ~400 km along the island chain changes composition systematically and synchronously, representing a replenishment of the plume head by a distinct mantle flavour on timescales of 3-5 Myr. These low-frequency compositional changes are also recorded by individual volcanoes, and comprise a sequence of closely-spaced isotopic trajectories. Each trajectory is maintained for ~1 Myr and is preceded and followed by ~0.3 Myr transitions to magmas with distinct isotope ratios. Relatively sharp transitions between periods of sustained isotopic stability require discrete yet coherent heterogeneities rising at speeds of ~100-200 km Myr^{-1} and extending for ~150 km vertically in the conduit. The long-term synchronous changes require larger scale isotopic domains extending ~600 km vertically through in the plume stem. These observations demonstrate that plumes can chemically "pulse" over short and long-timescales reflecting the characteristics and recycling history of the deep mantle.

1. Introduction

The mantle forms ~99% of the silicate Earth, so its composition and evolution are profoundly important in defining all aspects of Earth processes. Volcanic rocks provide constraints on how the composition of the mantle develops through mixing and recycling. In particular, insights into the deeper mantle can be gleaned through intra-plate volcanism generated by partial melting of ascending plumes. To determine the scale on which different compositions exist, we need to assess how material fed through the plume changes with time and with position across the volcanic province. For example, chemical and isotopic differences within Pacific volcanic islands are observed to be spatially separate, which may indicate that mantle components remain isolated during ascent (Abouchami et al., 2005; Farnetani and Hofmann, 2010; Huang et al., 2011; Jackson et al., 2014). However, there is the potential for these spatial isotopic variations to be generated by the thermal structure of the plume. This could take the form of differential sampling of heterogeneities with the depth or extent of melting ((Jones et al., 2017; Ren et al., 2005)), or by selective sampling of larger-scale heterogeneities by local melt transport systems (Shorttle et al., 2013).

Fig. 1 *Location of the Canary Islands with bathymetry surrounding the archipelago.*

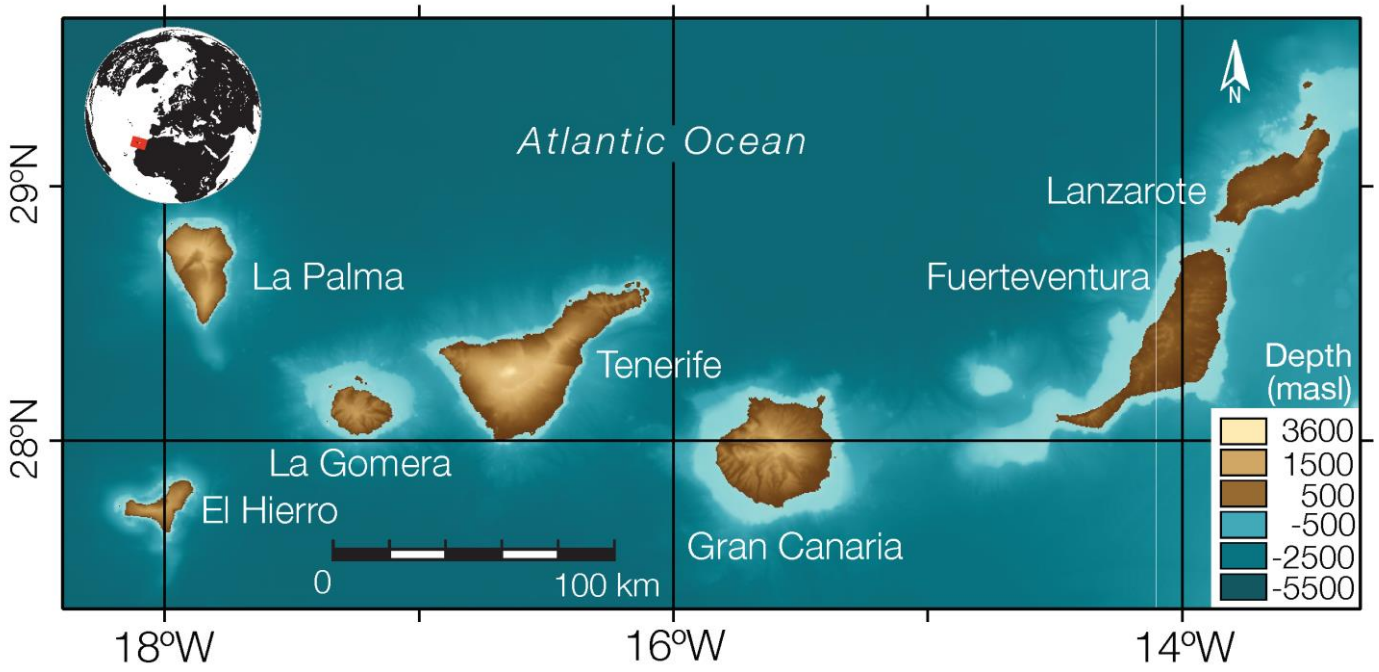

While there is clear evidence of spatially organised components in plume output (Genske et al., 2016; Peate et al., 2010), temporal changes in mantle chemistry are less obvious (Barker et al., 2010; Hoernle et al., 1991), chiefly due to the lack of exposed volcanic rocks with well-constrained ages that span sufficiently long time periods. Most investigations of well-dated volcanic successions typically span <300 Kyr (Blichert-Toft et al., 2003; Marske et al., 2007). Long-term changes in the Canary plume were recognised by (Hoernle and Schmincke, 1993) who identified periods of 2-5 Myr with distinct major and trace element characteristics during the ~15 Myr activity on Gran Canaria. Their study proposed that these cycles of volcanism related to variable melt extraction from heterogeneities or "blobs" rising in the Canary plume, with magmatic hiatuses between cycles taken to correspond with entrained material or melt-depleted blobs beneath a volcanic centre. Similar 3-5 Myr fluctuations were identified in the 11 Myr isotopic record of Icelandic Tertiary magmatism by (Kitagawa et al., 2008).

Determining the scale and shape of heterogeneities in the source of plumes during ascent is important in understanding the origin and dynamics of mantle mixing (Farnetani et al., 2018). The duration of isotopic perturbations observed in volcanic sequences has provided some constraints on the dimensions of heterogeneities (e.g. Blichert-Toft et al. (2003); Chauvel et al. (2012); Marske et al. (2007)), while U-series disequilibria (Bourdon et al., 2006; Sims et al., 1999) and thermal propagation (Ballmer et al., 2011; Parnell-Turner et al., 2014) provide some constraints on the rate of solid mantle upwelling.

To evaluate large-scale chemical variations emerging from the deep mantle we measured high-resolution Pb isotopes of the Tenerife volcanic system within the Canary Islands (Fig. 1): an archipelago marking the surface expression of the Canary mantle plume. Shorter timescale fluctuations are examined using an accurately dated and continuous volcanic stratigraphy spanning circa 2 Ma. From this we extend the findings to encompass volcanism across the plume head through the last 15 Myr. Pb isotopes are chosen as they have a very high measurement precision relative to the range of isotope ratios generally found in

the mantle: effectively they have around ten times greater resolution than other radiogenic systems such as Sr and Nd. Canary Sr and Nd isotopes do vary (e.g. Hoernle et al 1991) but not on a scale where subtle changes in the mantle source can be constrained. With three radiogenic ratios, $^{206}Pb/^{204}Pb$, $^{207}Pb/^{204}Pb$ and $^{208}Pb/^{204}Pb$, that record fractionation between Pb, U and Th during Earth evolution (expressed as $\mu = {}^{238}U/^{204}Pb$, $\omega = {}^{232}Th/^{204}Pb$ and $\kappa = {}^{232}Th/^{238}U$), Pb isotopes are a powerful tool to investigate fluctuations in mantle composition.

2. Samples, analysis and data selection

Felsic and basaltic rocks with well-constrained ages were sampled across Tenerife. Double spike Pb isotope data for 120 of these felsic and basaltic samples are presented in Tables 1 and 2 respectively. Fresh pumice fragments, obsidian and phonolite lava were collected from felsic units in the Bandas del Sur and the Costa Adeje pyroclastic sequences to span the last 1.84 Ma (Brown et al., 2003; Dávila Harris, 2009). Multiple samples of juvenile material were taken from many of the felsic pyroclastic units. Basaltic samples include basanites, tephrites, and phono-tephrites from the most recent lavas through to the 9-11 Ma Roque del Conde sequence. To increase the temporal coverage, quenched basaltic material and cumulate phases found in juvenile cognate cumulate nodules (Stock et al., 2012) were separated and analysed. These separates are denoted by the "nodule" suffix in Table 2. Melt-bearing nodules were collected from lapilli-tuff-breccias in four felsic eruptive units and consequently provide a direct comparison between coexisting basaltic and felsic magmas through the pyroclastic sequence. Taken together the felsic and basaltic eruptions provide a relatively continuous record of volcanism younger than 2 Ma, despite the reducing exposure concomitant with age. However in the period 1.0 – 1.3 Ma there are no exposed eruptive units. This could relate to a hiatus in volcanic productivity, but evidence from south west Tenerife indicates the gap may reflect the removal of exposed material by a landslide (Dávila Harris, 2009).

Rocks were prepared by initially crushing inside a plastic envelope using a non-torque press. Crushed material was then separated to 0.5-1.0 mm chips using a Teflon sieve set. This fraction was repeatedly cleaned with in ultra-pure water in an ultra-sonic bath. Cleaned rock-chips were then purified during a microscopic examination. Around 0.3 g of quenched melt from each cognate cumulate nodule was picked from the 0.5-1.0 mm fraction for isotopic analysis. All samples were leached for 30-40 min in 4M HCl at 200°C prior to Pb separation using HBr-HCl anion exchange columns. Pb isotope ratios were measured by a Thermo Neptune MC-ICP-MS at the University of Southampton UK, using a double spike run of each sample to correct for instrumental mass fractionation. The ^{207}Pb-^{204}Pb SBL74 spike (Taylor et al., 2015) was added such that $^{204}Pb_{sample}/^{204}Pb_{spike}$ was 0.09±0.03. Procedural blanks range between 30-95 pg Pb. NBS SRM 981 values achieved during the measurement period were $^{206}Pb/^{204}Pb$ = 16.9404 ±32, $^{207}Pb/^{204}Pb$ = 15.4969 ±32, $^{208}Pb/^{204}Pb$ = 36.7149 ±90 (2sd; n=44).

Fig. 2 *$^{206}Pb/^{204}Pb$ - $^{207}Pb/^{204}Pb$ for Tenerife volcanics comparing double spike data from this study with traditional f = constant data and Tl-spiked data (GeoRoc). Roque del Conde sample TF51 from Gurenko et al. (2006) is included in double spike data set.*

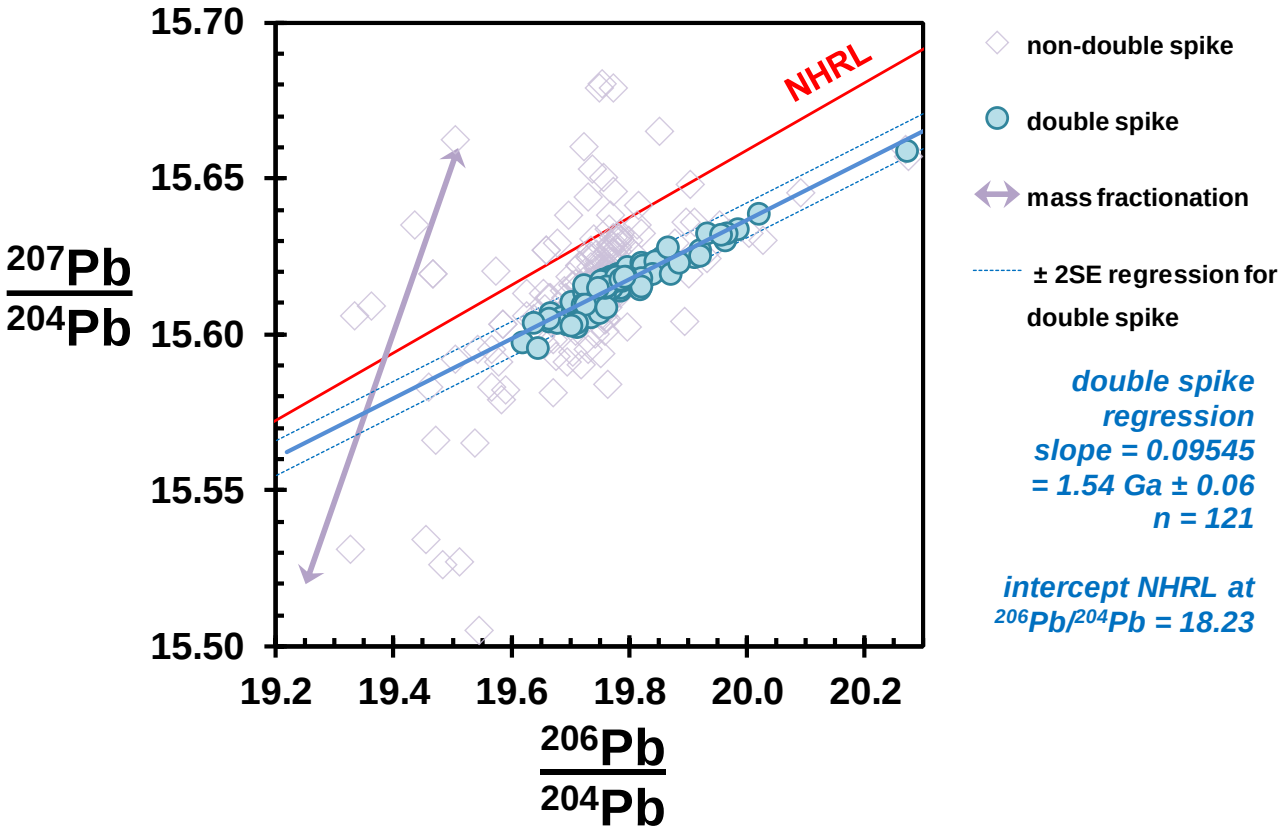

Pb isotopes were measured on between 2 and 7 juvenile fragments in 19 of the 28 felsic units. In these replicated units, 18 of the 19 resulted in the Pb isotopes falling within the analytical reproducibility quoted above – effectively the data from each unit defining an error ellipse. A sample from Montaña Blanca phase 7 (sample TF394, Table 1) was measured to test the anomalous Pb isotope ratios determined for this eruptive phase by Wiesmaier et al. (2012). Our phase 7 analysis was found to be within double spike error of our other three Montaña Blanca analyses indicating Pb isotopic homogeneity in this unit.

These data demonstrate the isotopic homogeneity of the felsic melt during an eruption, but also verify the uncertainty parameters for the double spike analysis of rock samples rather than standard solutions. Furthermore, this reproducibility justifies using an average isotope ratio for each felsic unit. An effect of averaging data falling within analytical error is to effectively increase the measurement precision by a factor of $1/\sqrt{n}$ which, in the case of the multiply analysed units, reduces the standard deviation by between 1.4 and 2.6 times.

Pb isotope data are presented and plotted as measured values rather than age-corrected values. This is preferable as it enables a direct comparison between historic lavas and eruptions >1 Ma without recourse to forward-modelling the older mantle source compositions. Measured values also provide consistency between high-precision data in this study and other data with incomplete Pb-Th-U concentration data. The

effects of age correction at 1.84 Ma are $^{206}Pb/^{204}Pb < 0.010$ and $^{208}Pb/^{204}Pb < 0.012$ which equate to a reduction in $\Delta^{207}Pb/^{204}Pb$ and $\Delta^{208}Pb/^{204}Pb$ of < 0.12 units.

To increase the age and spatial coverage of Pb isotope data, selected non-double spike analyses published from Tenerife were used. These data are factorised to equate the reported NBS SRM 981 values with the poly-spike average NBS 981 (Taylor et al., 2015). Data acquired by MC-ICP-MS procedures (Tl-spike or sample-standard bracketing) are preferred, although this has imprecision equivalent to ~3 times the double spike method.

For areas where double spike or MC-ICP-MS data is not available, selected thermal ionisation mass spectrometry (TIMS) data can potentially be utilised. The TIMS correction procedure assumes a constant fractionation factor (*f*) for all samples based on the average value achieved for the repeated measurement of NBS SRM 981. This exposes results to an array of fractionation-dependent issues related to filament temperature, sample load and Pb-ionisation suppression due to the presence of residual matrix. TIMS and non-double spike data for Tenerife are compared with the high precision data in Fig 2. The double spike data forms a tight linear trend in $^{206}Pb/^{204}Pb$ and $^{207}Pb/^{204}Pb$ with a relatively consistent position below the northern hemisphere reference line (NHRL) at $\Delta^{207}Pb/^{204}Pb \sim -2$, while non-double spike data are variably scattered about this line along a mass fractionation vector. If we assume that all samples from Tenerife should lie along this $^{206}Pb/^{204}Pb$ and $^{207}Pb/^{204}Pb$ trend, then any deviation of a sample from this trend would be proportional to the inaccuracy of the original instrumental mass fractionation correction. In this way the original data can be projected along a mass fractionation line to intercept the $^{206}Pb/^{204}Pb$:$^{207}Pb/^{204}Pb$ regression line. General equations to calculate corrected $^{206\text{-}207\text{-}208}Pb/^{204}Pb$ are provided in the Supplementary Information. Only data for Tenerife lavas where double spike analyses are not available are corrected by this method.

3. Temporal isotopic variation in Tenerife

We examine changes in mantle composition using $\Delta^{207}Pb/^{204}Pb$ and $\Delta^{208}Pb/^{204}Pb$ and $^{208}Pb^{*}_{1500}/^{206}Pb^{*}_{1500}$ through the last 2 Myr on the island of Tenerife in Fig. 3. Both felsic (phonolite/trachyte) and basaltic (basanite/tephrite) volcanism were active during this period. The felsic volcanics record a progressive increase in $\Delta^{208}Pb/^{204}Pb$ and $^{208}Pb^{*}_{1500}/^{206}Pb^{*}_{1500}$ between 1.84 Ma and 1.5 Ma, followed by consistent ratios (~11 and 1.04 respectively) through to 0.5 Ma, before a smooth decline to ~0.15 Ma where the ratios are similar to the most recent eruptions (<9000 yrs). In contrast, $\Delta^{207}Pb/^{204}Pb$ is essentially constant, with all magmas lying below the NHRL at -1.9 (±0.5). The basaltic volcanics follow the same temporal pattern, but with slightly wider variations in $\Delta^{208}Pb/^{204}Pb$ and $^{208}Pb^{*}/^{206}Pb^{*}$.

Fig. 3 *$\Delta^{207}Pb/^{204}Pb$, $\Delta^{208}Pb/^{204}Pb$ and $^{208}Pb^*_{1500}/^{206}Pb^*_{1500}$ of felsic and mafic <2 Ma Tenerife volcanics. Each felsic point averages 1-6 measurements (see supplementary information). Grey lines represent the time-track of felsic magmatism. $\Delta^{207}Pb/^{204}Pb$ and $\Delta^{208}Pb/^{204}Pb$ represent $^{207}Pb/^{204}Pb$ and $^{208}Pb/^{204}Pb$ expressed as vertical deviation from the Northern Hemisphere reference line (NHRL). $^{208}Pb^*_{1500}/^{206}Pb^*_{1500}$ is the $^{208}Pb^*/^{206}Pb^*$ calculated by subtraction of MORB at 1500 Ma where:*

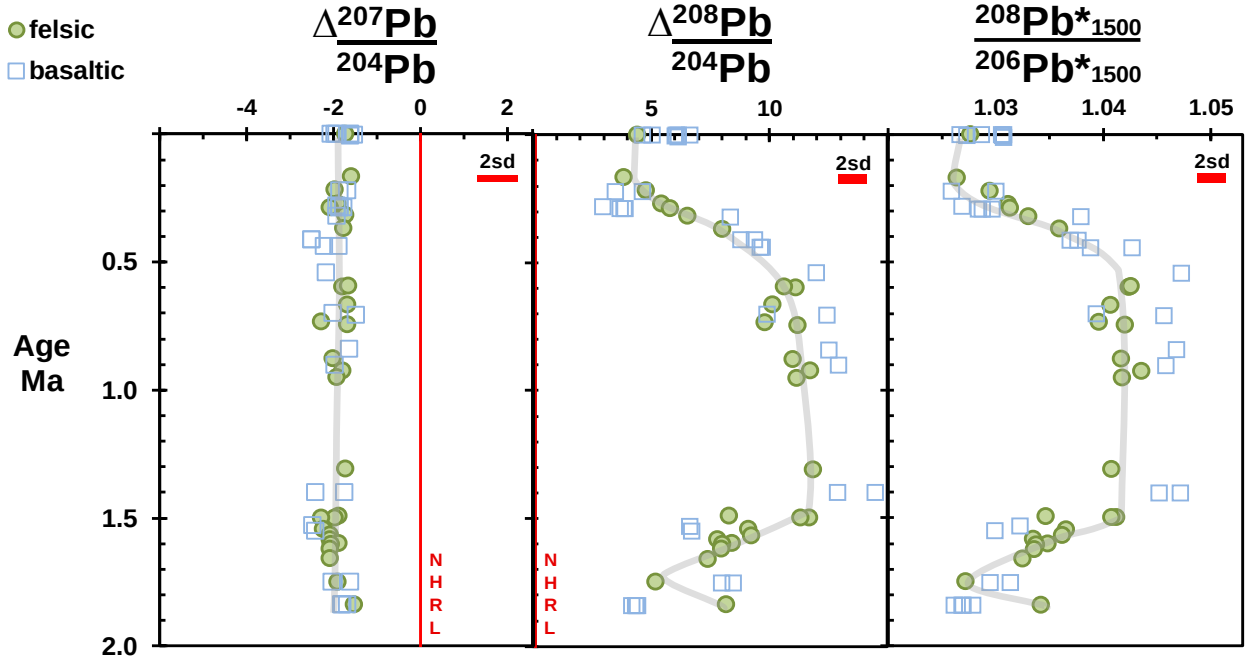

$(^{208}Pb/^{204}Pb_{sample} - ^{208}Pb/^{204}Pb_{MORB\ 1500})/(^{206Pb}/^{204}Pb_{sample} - ^{206}Pb/^{204}Pb_{MORB\ 1500})$. MORB at 1500 Ma is back calculated from MORB today with $^{206}Pb/^{204}Pb$ =18.275, $^{207}Pb/^{204}Pb$ =15.472, $^{208}Pb/^{204}Pb$ = 37.721 and assuming $^{232}Th/^{238}U$ = 3.10 and $^{238}U/^{204}Pb$ = 10.4 at 1500 Ma (Elliott et al., 1999; Thirlwall, 1997). The parameter $^{208}Pb^*_{1500}/^{206}Pb^*_{1500}$ is used instead of $^{208}Pb^*/^{206}Pb^*$ as it is found to be invariant along the $^{206}Pb/^{204}Pb$ - $^{208}Pb/^{204}Pb$ trends produced for Tenerife lavas.

Temporal variation in Pb isotopes is examined further in Figure 4. This shows that over the course of ~2 Myr felsic magmas define a remarkably coherent isotopic "loop" with sequential changes in $\Delta^{208}Pb/^{204}Pb$ and $^{206}Pb/^{204}Pb$. Following an increase in $\Delta^{208}Pb/^{204}Pb$ from 5 to 12 between 1.8 Ma and 1.5 Ma, $\Delta^{208}Pb/^{204}Pb$ remains consistent for ~1 Myr during which $^{206}Pb/^{204}Pb$ progressively increases. In the following ~0.3 Myr, $\Delta^{208}Pb/^{204}Pb$ declines from ~11 to ~4 at similar $^{206}Pb/^{204}Pb$, and remains at this composition to the present. Basaltic magmas show a similar and concurrent time-progressive pattern. Basaltic samples older than 1.55 Ma fall along a low $\Delta^{208}Pb/^{204}Pb$ trajectory. This is followed by a switch to a high $\Delta^{208}Pb/^{204}Pb$ trajectory between ~1.4 Ma and ~0.56 Ma which, like the felsic magmas, is characterised by a progressive increase in $^{206}Pb/^{204}Pb$. Basaltic magmas then revert to a low $\Delta^{208}Pb/^{204}Pb$ trajectory over ~0.3 Ma, again retaining a similar $^{206}Pb/^{204}Pb$. Since ~0.3 Ma the most recent basalt isotope compositions have remained along this Δ-trajectory but have decreased $^{206}Pb/^{204}Pb$. Therefore, despite these coordinated changes in felsic-basaltic magmas, the basalts have slightly more diverse and erratic isotope compositions compared to the smooth progressive changes in felsic lavas.

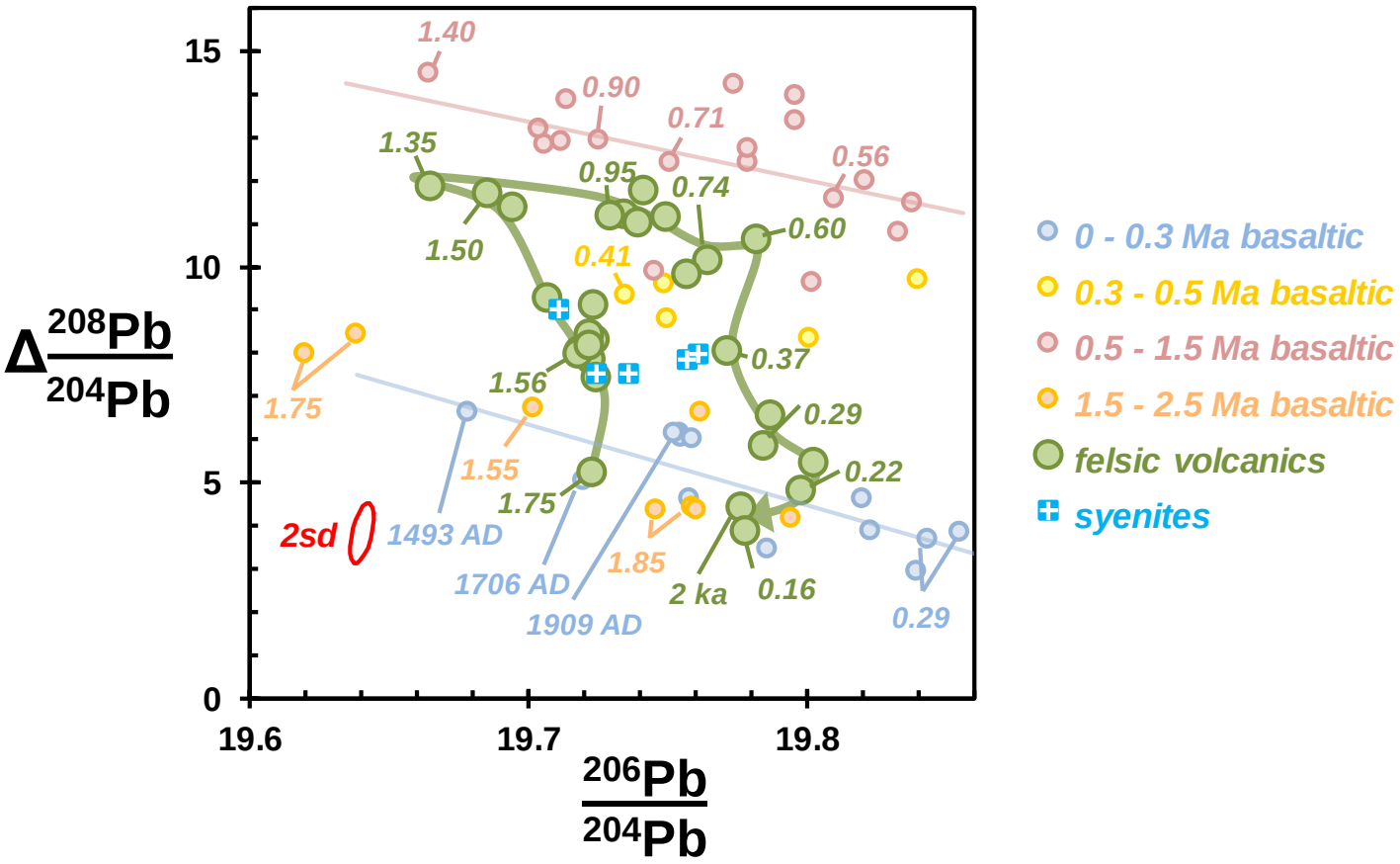

Fig. 4 *$^{206}Pb/^{204}Pb$ - $\Delta^{208}Pb/^{204}Pb$ for Quaternary Tenerife magmatism. Felsic points and time-track as for Fig. 3. Values are Ma unless specified. Basaltic lavas 0-0.3 Ma and 0.5–1.5 Ma are highlighted by red and blue linear regressions. Additional data for 0.5–1.5 Ma are from (Deegan et al., 2012). Syenite analyses are of accidental lithic clasts found in the Fasnia, San Juan and Morteros ignimbrites. See Table 2 for details.*

Figure 4 also shows the composition of 5 syenite clasts extracted from lapilli-tuff breccias in the Fasnia formation (0.29 Ma), San Juan ignimbrite (1.5 Ma) and the Morteros ignimbrite (1.75 Ma). These units all originate from the same Las Canadas volcanic centre as the recent felsic volcanism. Based on their hydrothermal alteration and angular appearance, they are likely accidental clasts, removed from the walls of the felsic magma reservoir during these Plinian eruptions. Notably, their Pb isotopes lie roughly in the centre of the felsic loop and, as a group, have more coherent isotope compositions relative to the juvenile material in their hosts.

4. Effects of a chemically fluctuating mantle plume

Basaltic eruptions occur approximately every 100-1000 years on Tenerife with volumes around 0.5 km^3.kyr during the last 200 kyr (Carracedo et al., 2007). Effusive felsic magmatism has a slightly higher eruption rate in this same period at 0.8 km^3.kyr (Carracedo et al., 2007). Major explosive felsic events occur every ~25 kyr years through the last 1.8 Myr (Dávila Harris, 2009) with the total erupted material equating to around 0.3 $km^3.kyr^{-1}$ (Edgar et al., 2007). Frequent basaltic volcanism during such a prolonged time span is consistent with a steady throughput of basic magma from the mantle. A similar frequency of felsic eruptions indicates this basic magma is also fed through a fractional crystallisation reservoir. As the felsic rocks on Tenerife contain ~4 times the Zr content of the basaltic rocks (1100 ppm vs 280 ppm) it implies

around 75% crystallisation is required to generate the phonolitic magma. Hence 1.1 $km^3.kyr^{-1}$ of total felsic magma erupted (effusive and explosive) is likely to have been distilled from ~4.4 $km^3.kyr^{-1}$ of basaltic magma. So in any given time period, both felsic and basaltic outputs represent an integration of mantle compositions, but felsic magma potentially representing a larger volume of primitive melt than the basaltic magma. Progressive crystallisation generating the felsic liquid may to some extent retard the surface appearance of a change in mantle composition. However, given the throughput required by the felsic system and the frequency of explosive events, this is likely to be on timescales <20 kyr. This felsic "crystallisation filter" may also aggregate heterogeneities present in small melt batches arriving from the mantle (e.g. (Cousens et al., 1990), and may result in the smoother isotopic changes in felsic magmas through the last 1.8 Myr (Figs. 3 and 4).

The observation that the basaltic and felsic magmas have approximately the same time-equivalent isotope ratios is important because it indicates that melting of pre-existing cumulates (Turner et al., 2017; Wiesmaier et al., 2012) does not significantly affect Pb isotopes during magma storage. Effectively the felsic melts appear to change their overall Pb isotope ratios in response to fluctuations in the composition of mantle-derived basaltic magmas.

Turner et al. (2017) noted that Pb isotopes appear to correlate with SiO_2 in recent Tenerife volcanism. They observed that higher $^{206}Pb/^{204}Pb$ in the more phonolitic lavas was concomitant with $^{230}Th/^{238}U$, $^{231}Pa/^{235}U$ and $^{226}Ra/^{230}Th$ activities simultaneously reaching equilibrium. Based on an assumed Pb isotope composition for syenite ($^{206}Pb/^{204}Pb$ =19.95) Turner et al., (2016) suggested that $^{206}Pb/^{204}Pb$ was increased in the felsic magmas following partial melting of crustal syenites.

However, crustally-derived syenite clasts found in the associated pyroclastic sequence (Fig. 4) actually have a *lower* $^{206}Pb/^{204}Pb$ than the recent felsic volcanics and are more similar to the historical basalt compositions. As these syenites represent felsic accumulation within the last ~2 Myr beneath the Las Cañadas caldera, they are the most likely crustal assimilant. This again indicates that Pb isotopes are not significantly affected by crustal melts and that the isotopic differences between the felsic and mafic magmas are dominantly related to a changing mantle source composition and magma throughput. However, this does not preclude limited melting of syenites or assimilation of ageing felsic crystal mush in the magma reservoir (Sliwinski et al., 2015) which is required by the U-series disequilibrium systematics (Turner et al., 2017). The effect of restricted assimilation of melted syenites with compositions in the centre of the isotopic "loop" would be to moderate the $\Delta^{208}Pb/^{204}Pb$ in the felsic magmas relative to the basalts. This may explain why the felsic units between 1.5 - 0.5 Ma have a slightly lower $\Delta^{208}Pb/^{204}Pb$ (10 – 12) relative to the contemporaneous basaltic magmas (12 - 14).

Isotopic changes observed for the last 1.84 Myr on Tenerife (Fig. 3) identify that high $\Delta^{208}Pb/^{204}Pb$ trajectory magmas erupted for a period of ~1 Myr, but the changes to and from this composition were progressive and lasted ~0.3 Myr. If basaltic melts are transferred from the asthenosphere at ~20-200 $m.yr^{-1}$ (Stracke et al., 2006), with the ~70 km transit to the upper crust taking < 4 kyr, then these isotopic transitions are likely to reflect the progress of plume heterogeneities rising into the melt generation zone

at the top of the plume stem. Because the transition between trajectories is progressive, it implies that for a period of time melt from the incoming heterogeneity is integrated with melt from the outgoing one, with ~0.3 Myr being the time taken for the new $\Delta^{208}Pb/^{204}Pb$ to displace the signature of the old. As such this transition time should be proportional to the plume ascent rate.

Progressively co-varying $^{206}Pb/^{204}Pb$ and $^{208}Pb/^{204}Pb$ during the timespan of a $\Delta^{208}Pb/^{204}Pb$ trajectory (Fig. 4) must arise from gradients in μ and ω, which could stem from variable proportions of metasomatic pyroxenite or eclogite within peridotite (e.g. (Gurenko et al., 2009; Jackson et al., 2012)). These progressive changes in $^{206}Pb/^{204}Pb$ (as well as $^{207}Pb/^{204}Pb$ and $^{208}Pb/^{204}Pb$) may be a response to a variation in the relative contribution of these heterogeneities to the isotope composition of the magma. Such changes could result from a fluctuation in the proportion of melting in response to pressure (e.g. (Sims et al., 2013)) or thermal perturbations (Ito and Mahoney, 2005) potentially generated by a horizontal movement in the plume stem. However, an important feature of the Pb-isotope loop is that as it passes from one $\Delta^{208}Pb/^{204}Pb$-trajectory to another, the volcanics retain the $\sim^{206}Pb/^{204}Pb$ of the preceding $\Delta^{208}Pb/^{204}Pb$-trajectory. This suggests that μ and ω variation is present in the mantle on a finer scale and is effectively superimposed on and across the $\Delta^{208}Pb/^{204}Pb$ heterogeneities. Hence, it is likely that the isotopic transition between two $\Delta^{208}Pb/^{204}Pb$-trajectories relates to a general shift in the composition of the rising mantle whereas $^{206}Pb/^{204}Pb$ could respond to changing intensive parameters.

Fig. 5 *$^{206}Pb/^{204}Pb$ - $^{208}Pb/^{204}Pb$ for Tenerife basaltic volcanics. Additional data for Tenerife are from (Deegan et al., 2012). Anaga and Teno isotopes from (Simonsen et al., 2000) and sample TF328 from Table 2. Anaga and Teno isotopes are re-corrected for mass fractionation using the method outlined in section 2 and the Supplementary Information. Dashed line represents evolution of ocean crust following U-addition during alteration and U-Pb loss during subduction at 1.5 Ga. Diamonds represent evolution of μ = 14.3 & ω = 56; μ = 16.3 & ω = 58.6. Solid grey lines represent evolution of compositions marked by diamonds assuming constant κ but μ increased up to 10%. Model parameters after (Kelley et al., 2005) are:* ***Stage 1****; MORB today $^{206}Pb/^{204}Pb$ = 18.275, $^{207}Pb/^{204}Pb$ = 15.472, $^{206}Pb/^{204}Pb$ = 37.721 taken back 1.5 Ga using μ = 10.4 and ω = 36.4 κ = 3.10; MORB is (Gale et al., 2013; Workman and Hart, 2005) value of $^{206}Pb/^{204}Pb$ = 18.275 taken on the NHRL. κ estimate for 1.5 Ga from (Elliott et al., 1999).* ***Stage 2a****: resultant isotopes are evolved forward by 1.5 Ga using μ = 10.4-18.2 and ω = 51-6.* ***Stage 2b****: compositions at μ = 14.3 and μ = 16.3 are evolved forward 1.5 Ga assuming Pb is removed (or U & Th are enriched) by up to 10% (κ = constant at 3.9 and 3.6 respectively)*

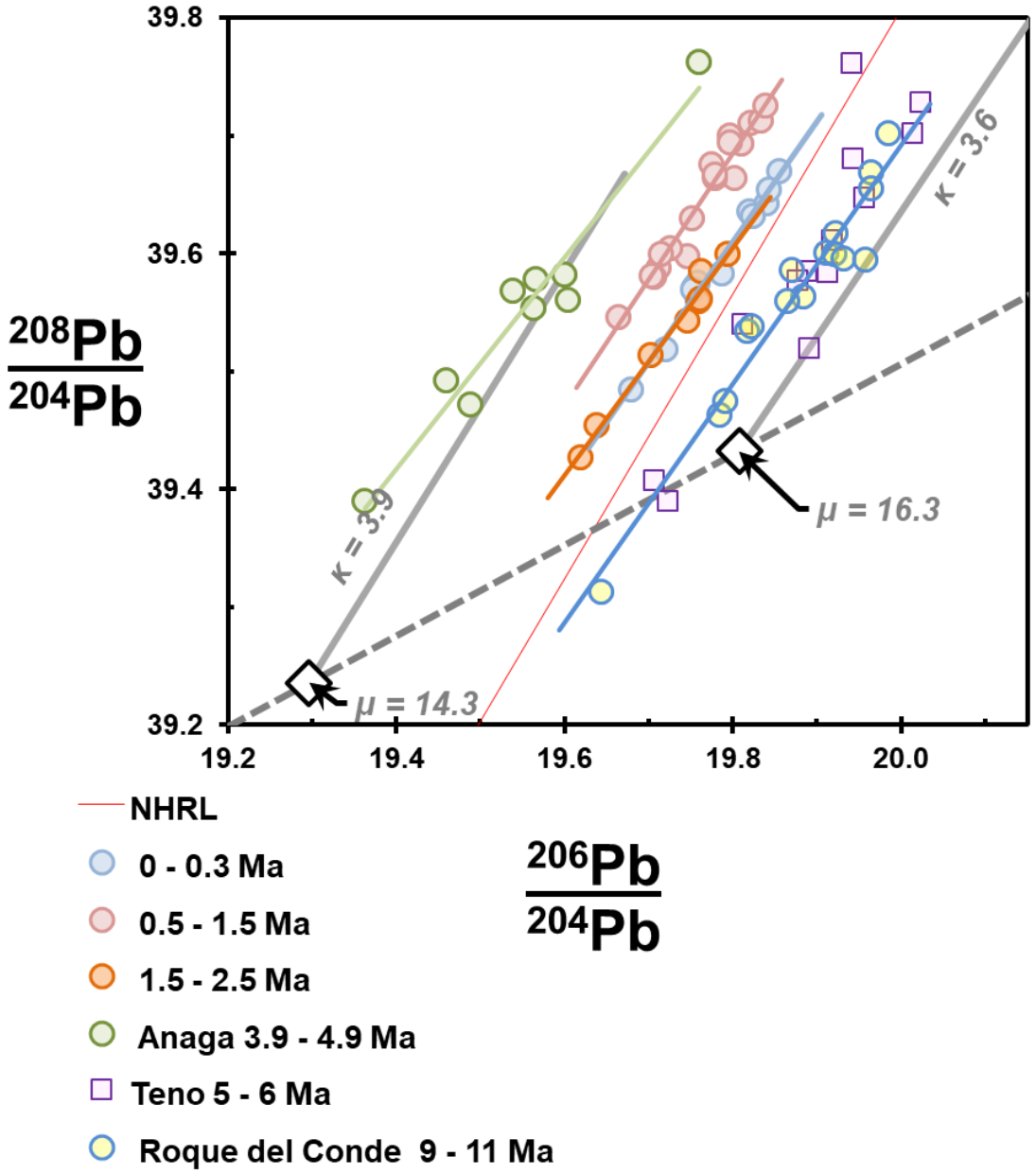

As noted above, while $\Delta^{208}Pb/^{204}Pb$ systematically changes through time, $\Delta^{207}Pb/^{204}Pb$ remains consistent for all Tenerife volcanics, regardless of age, magma composition or location. Nevertheless, our high-precision analyses show that $\Delta^{207}Pb/^{204}Pb$ shows a slight but progressive decrease with higher $^{206}Pb/^{204}Pb$ (Fig. 2). If this slope represents an isochron, it suggests that μ was variably increased by an event at ~1.5 Ga; possibly as a result of U-gain during ocean crust alteration or subsequent Pb-loss during subduction at this time (e.g. (Beier et al., 2008; Deegan et al., 2012; Hoernle et al., 1991; Simonsen et al., 2000; Thirlwall, 1997)).

Evaluation of the Pb Isotopic variation on Tenerife is extended to cover the last ~11 Myr in Figure 5. Taken as a whole, the data forms a broad $^{208}Pb/^{204}Pb$-$^{206}Pb/^{204}Pb$ array crossing the NHRL at a shallow angle. In detail, it can be observed that this array is composed of *en-echelon* $\Delta^{208}Pb/^{204}Pb$-trajectories, each representing about 1 Ma of volcanism. These *en-echelon* Δ-trajectories effectively disperse the $^{208}Pb/^{204}Pb$-$^{206}Pb/^{204}Pb$ array, implying that they result from an element-redistribution event superimposed on a pre-existing variable κ-heterogeneity. However, as the $^{207}Pb/^{206}Pb$ gradients of each Δ-trajectory are within error of each other and the overall $^{207}Pb/^{206}Pb$ slope (Fig. 2), the interval between generation of the Δ-trajectories and κ-heterogeneities should be <~150 Ma.

It should also be noted from Figure 5 that if the *en-echelon* $\Delta^{208}Pb/^{204}Pb$-trajectories are extrapolated back to $^{206}Pb/^{204}Pb$ of ~18.2, they project above the NHRL to $\Delta^{208}Pb/^{204}Pb$ between 20 and 50. This is significantly different to Atlantic MORB at 18.2 (-10 to +10) and to altered Atlantic MORB (<<-10). As such, it is difficult to reconcile the $\Delta^{208}Pb/^{204}Pb$-trajectories with interaction between high $^{206}Pb/^{204}Pb$ plume-derived melts and Atlantic lithospheric mantle or ocean crust. Consequently, it seems likely that the high and low $^{206}Pb/^{204}Pb$ components controlling these trends are a result of radiogenic development in the asthenosphere.

5. Synchronous behaviour across the plume head

Having considered the frequency and isotopic nature of heterogeneities, we can investigate how they present themselves along the ~400 km of active volcanism and on longer timescales. Isotopic data from the other Canary Islands in Figure 6(a) indicates they form similar *en-echelon* arrays to those of Tenerife. However, an important observation is that the higher and lower $\Delta^{208}Pb/^{204}Pb$-trajectories of Tenerife are roughly coeval with matching trends on the other islands. This is illustrated in Fig. 6(b) which shows that between 17-13 Ma $^{208}Pb^*_{1500}/^{206}Pb^*_{1500}$ was ~1.02, followed by ~5 Myr of eruptions with ~1.0. Compositions then switched sharply to ~1.08 in the period 5-3 Ma, before $^{208}Pb^*_{1500}/^{206}Pb^*_{1500}$ progressively declined to 1.0-1.02 in recent volcanism.

Fig. 6 (a) *$^{206}Pb/^{204}Pb$ vs $\Delta^{208}Pb/^{204}Pb$ for Canary plume coded by age and volcanic centre. Lines show equal $^{208}Pb^*_{1500}/^{206}Pb^*_{1500}$ trajectories* ***(b)*** *$^{208}Pb^*_{1500}/^{206}Pb^*_{1500}$ variation through time for the Canary plume. Symbols represents average isotope ratio and average eruption age. Horizontal and vertical bars represent the range of isotope ratio and duration of activity respectively. Grey line tracks time-progressive change in Pb isotopes. Using $^{208}Pb^*_{1500}/^{206}Pb^*_{1500}$ (see Fig. 3) minimises changes in $^{208}Pb^*/^{206}Pb^*$ with $^{206}Pb/^{204}Pb$ along $\Delta^{208}Pb/^{204}Pb$ trajectories.* ***(c)*** *$^{208}Pb^*_{1500}/^{206}Pb^*_{1500}$ variation as for (b) but the ages include the transit time of asthenosphere flow from the plume centre (assumed as El Hierro) to beneath each volcanic centre, and for plate movement relative to the plume using the equation below. This figure shows an outflow velocity v_p of 160 km.Myr^{-1} with a plate velocity v_t of 10 km.Myr^{-1}.* ***(d)*** *as for (b) but outflow is 40 km.Myr^{-1}.*

$$a_c = a_e + \frac{l - (a_e . v_t)}{v_p}$$

where:

$a_c = age\ since\ leaving\ plume\ centre,$

$a_e = eruption\ age,$

$l = distance\ from\ plume\ centre,$

$v_t = plate\ velocity,$

$v_p = velocity\ of\ plume\ outflow$

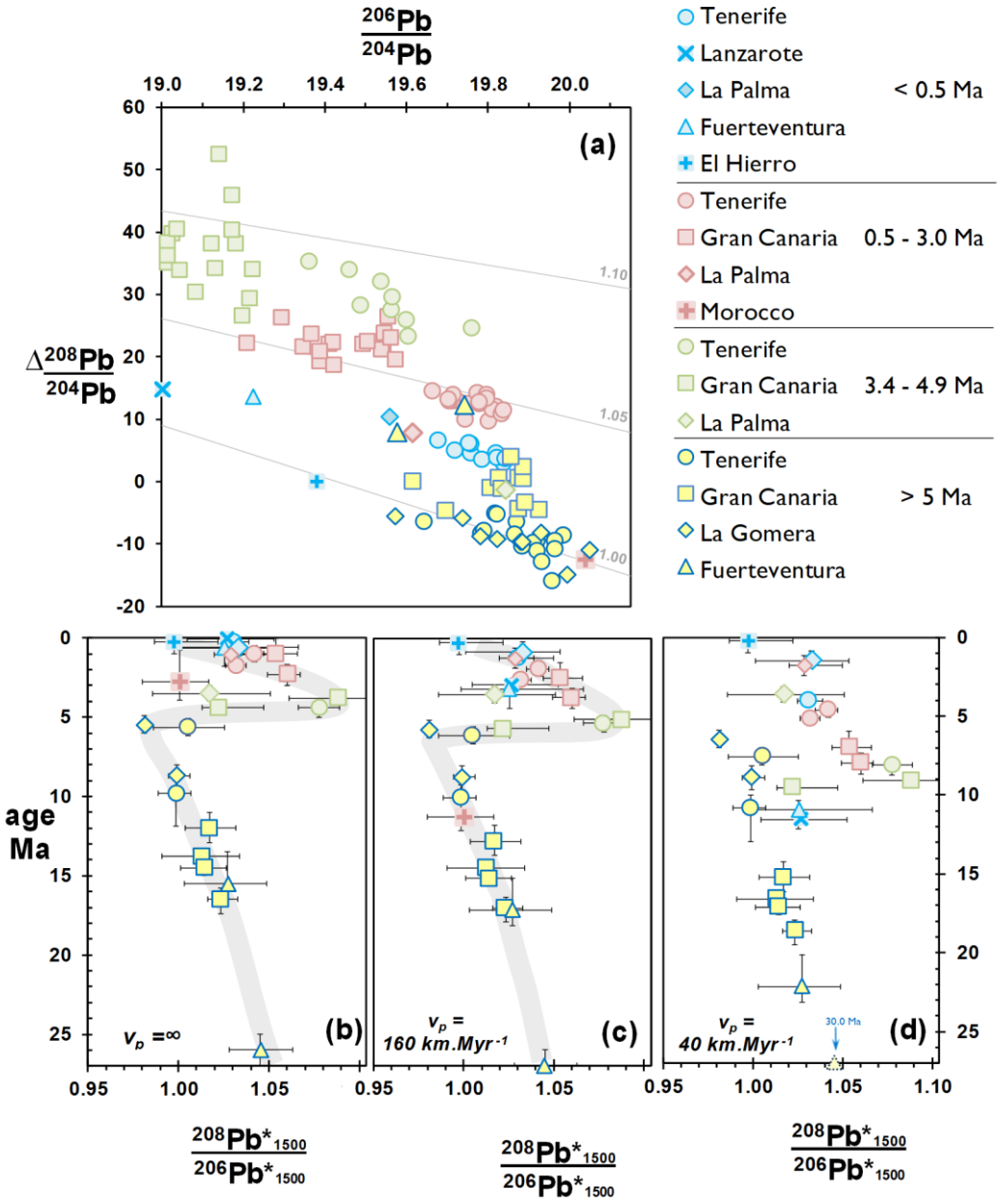

As Figure 6(b) records isotope composition at the age of eruption, it effectively assumes that there is no time delay between mantle reaching the top of the plume and producing melts beneath each volcano i.e. an infinite speed of outflow, or the plume stem is wider than the geographical spread of volcanism. The concept of a broad plume beneath the Canaries is not new, and is a key feature of the Hoernle and Schmincke (1993) "blob" model. Their model portrays ~300 km diameter upwelling, with outflow directed to the east or north east of the islands while continuously rising. Geophysical data and models provide some support for this (Bonnin et al., 2014; Mériaux et al., 2015) with a semi-continuous ~300 km wide low velocity region extending ~1800 km to the north east of the Canaries (Miller et al., 2015).

If the plume outflow velocity to the north-east is ~160 km.Myr^{-1}, then material at the centre of the plume stem will take 2-3 Myr to transit from El Hierro to Lanzarote. Effectively there is a lag between the emergence of a heterogeneity above the stem and its appearance downstream. This is to some extent affected by the easterly movement of the African plate at ~10 km.Myr^{-1} which has moved volcanoes further from the plume with time, such that distal volcanoes were once closer to the stem. To examine this lag effect on the isotopic signal, outflow rates of 160 km.Myr^{-1} and 40 km.Myr^{-1} are modelled in Figure 6(c) and (d) respectively. The age-isotope profile of the faster rate is not significantly different from the infinite case, other than separating La Palma and the more easterly islands at ~4-5 Ma. Notably, the 40 km.Myr^{-1} outflow (Fig. 6(d)) disturbs any systematics within the age-isotope profile. The 40 km.Myr^{-1} profile appears roughly as two trends with higher and lower $^{208}Pb^*_{1500}/^{206}Pb^*_{1500}$ that overlap in time. Potentially this could mark the passage of two sequentially emerging isotopic domains being sampled in the same time period at different distances from the plume centre. However, this does not fit with the observation that in the 40 km.Myr^{-1} profile the older isotope trend (25-5 Ma. in Fig. 6(d)) would have to emerge at the volcanic centres closer to the plume (La Gomera and NW Tenerife) after the younger trend is observed at more distal centres (NE Tenerife and Gran Canaria).

Hot asthenosphere originating from the Canary Plume has been suggested as an origin for Pliocene-Pleistocene volcanics in Morocco. Support for this comes from the least crustally contaminated of these lavas which are isotopically similar to the Canary plume (Duggen et al., 2009). Fig. 6 plots the average of these Moroccan lavas, limited to samples with $\Delta^{207}Pb/^{204}Pb < -1.0$ and $^{87}Sr/^{86}Sr < 0.7034$ to minimise crustal effects. In terms of $\Delta^{208}Pb/^{204}Pb$ and $^{208}Pb^*_{1500}/^{206}Pb^*_{1500}$ it is similar to the Canary Islands between ~6 and 15 Ma, and is quite

different from the Canary volcanics of equivalent age (~2.7 Ma). However, when modelled for lateral asthenosphere flow at 160 km.Myr^{-1} and the ~1300 km distance, the Moroccan lavas are found to have a similar age-composition relationship to the Canaries (Fig. 6(c)). This relationship is observed in models for any flow-rate between 100-200 km.Myr^{-1}.

Volcanism on the Canary Islands as a whole has been continuous through the last ~18 Ma, except for an apparent hiatus between ~6 and 9 Ma (Hoernle and Schmincke, 1993). The lack of magmatism in this period could be related to the rising plume lacking fusible material, or being cooler (e.g, (Ballmer et al., 2013)). For an outflow rate of 110 km.Myr^{-1}, this hiatus roughly equates to a current distance of 700-1000 km from the plume. Interestingly, this range spans a region with higher velocity extending from ENE of the Canaries to beneath western Morocco identified by (Miller et al., 2015).

These observations imply that all volcanic centres across >400 km experienced *coordinated* changes in $\Delta^{208}Pb/^{204}Pb$ and $^{208}Pb^*_{1500}/^{206}Pb^*_{1500}$, and these changes occurred *irrespective* of the absolute $^{206}Pb/^{204}Pb$ or $^{208}Pb/^{204}Pb$. In other words the similar $\Delta^{208}Pb/^{204}Pb$ for Tenerife and Gran Canaria in the same time interval (Fig. 6(a)) contrasts with the lower $^{206}Pb/^{204}Pb$ observed for Gran Canaria. This decoupling of $\Delta^{208}Pb/^{204}Pb$ from $^{206}Pb/^{204}Pb$ may be a product of a partial extraction of a short-length-scale high-$^{206}Pb/^{204}Pb$ heterogeneity in the vicinity of the plume stem. In contrast, the $\Delta^{208}Pb/^{204}Pb$ persists away from the plume stem as both the higher and lower $^{206}Pb/^{204}Pb$ heterogeneities lie along the same Δ-trajectory. Such large-scale coordination implies the plume head was replenished with rising mantle of similar $\Delta^{208}Pb/^{204}Pb$ composition through periods of 3-5 Myr. Furthermore, this coordination suggests that material is transferred upward and laterally from the plume centre at rates of >100 km.Myr^{-1}

Progressive isotopic changes observed through 3-5 Myr appear to be composed of individual volcanoes that have ~1 Myr periods with a distinct Δ-trajectory (e.g. Fig. 3 and 4). However, such distinctions remain within the long-timescale trend, which suggests between 3 and 5 broadly similar Δ-trajectories make up a larger-scale heterogeneity with similar κ (κ-heterogeneity).

6. Structure of heterogeneities in the plume

Temporal isotopic fluctuations in plume volcanics should reflect the disposition and composition of heterogeneities rising through the plume stem. Based on our observations, we can potentially place some constraints on the size and form of these heterogeneities in relation to plume dynamic models.

In its simplest form, a heterogeneity can be modelled as a cylinder of mantle (Blichert-Toft et al., 2003), rising and displacing a pre-existing plug out of the melting zone and into the plume outflow (Fig. 8(a)). Such a plug flow could be generated by a non-linear rheology in a conduit with limited attenuation at the edges of the conduit (e.g. (Massmeyer et al., 2013)). Based on P-wave velocity models, the vertical distance between the onset of melting and the lithosphere is between 40 and 65 km for Reunion, Canary, Galapagos, and Hawaii (Fontaine et al., 2015; Gibson et al., 2015; Miller et al., 2015; Rychert et al., 2014; Rychert et al., 2013). On this basis, for a plug of mantle to fully occupy a 50 km thick melting interval within the observed 0.3 Myr transition time requires an ascent rate of ~167 km Myr^{-1}. This is a simplistic estimate and if, for example, the melting zone was thinner the same transition time would represent a slower integrated ascent rate: for a melting interval of 30 km this reduces to 100 km Myr^{-1}. Similarly, a slower ascent would apply if the incoming isotope heterogeneity replaced the signal of the previous residual material before it had been completely displaced from the melt zone. This latter point is equivalent to the Pb isotope signal being overwhelmed by the incompatible element enriched magmas formed in a 15-30 km interval at the base of the melting column e.g. (Rudge et al., 2013).

The thickness of the melting interval is somewhat constrained by La/Y and Dy/Yb of Canary Islands magmas which require aggregate melts from the garnet and spinel facies mantle (Thirlwall et al., 2000). These rare-earth systematics indicate that 15% (±10%) of magma is sourced from ~5% melting of spinel peridotite, with the remaining sourced from <2% melting in garnet stability (> ~70 km). However, this is slightly at odds with the geophysical estimates of the lithosphere-asthenosphere boundary at depths between 60 and 80 km ((Martinez-Arevalo et al., 2013; Miller et al., 2015). S receiver function analysis suggests that melt-bearing low-velocity material extends to >150 km beneath all of the Canary Islands (Bonnin et al., 2014; Miller et al., 2015).

Lanzarote is 300-400 km from the putative centre of the plume, yet has experienced a significant eruption in 1730-6 and a smaller eruption in 1824. This testifies to melt production beneath, and geographically close to, this island. Plume mantle would need to be capable of generating significant melt volumes with compositions that are not dissimilar from the most incompatible element enriched magmatism found on the western Canaries. Therefore it is possible that plume outflow retains the thermal potential to generate melt through adiabatic upflow as well as outflow. It may also indicate that un-melted material is retained in the deeper levels of the plume outflow. Combining the geophysical and

geochemical observations, a schematic model of the Canary Plume dynamics are shown in Fig. 7.

Fig. 7 *(a) Schematic block diagram (a) showing the scale and directed outflow from the Canary mantle plume. Plume position and dimensions constrained after (Bonnin et al., 2014; Duggen et al., 2009; Farnetani and Hofmann, 2010; Geldmacher et al., 2005; Martinez-Arevalo et al., 2013; Miller et al., 2015). $\Delta^{208}Pb/^{204}Pb$ variation the plume and outflow is represented by the orange, red and yellow domains. (b) Horizontal section through the plume showing broadening and shoaling hot asthenosphere. Yellow domain within the plume may represent a cooler or melt-poor region (Bonnin et al., 2014; Miller et al., 2015): this part of the outflow may have been responsible for the lack of volcanism in the 9-6 Ma period. Stipple shown indicates the likely region of melt generation beneath the active volcanic centres.*

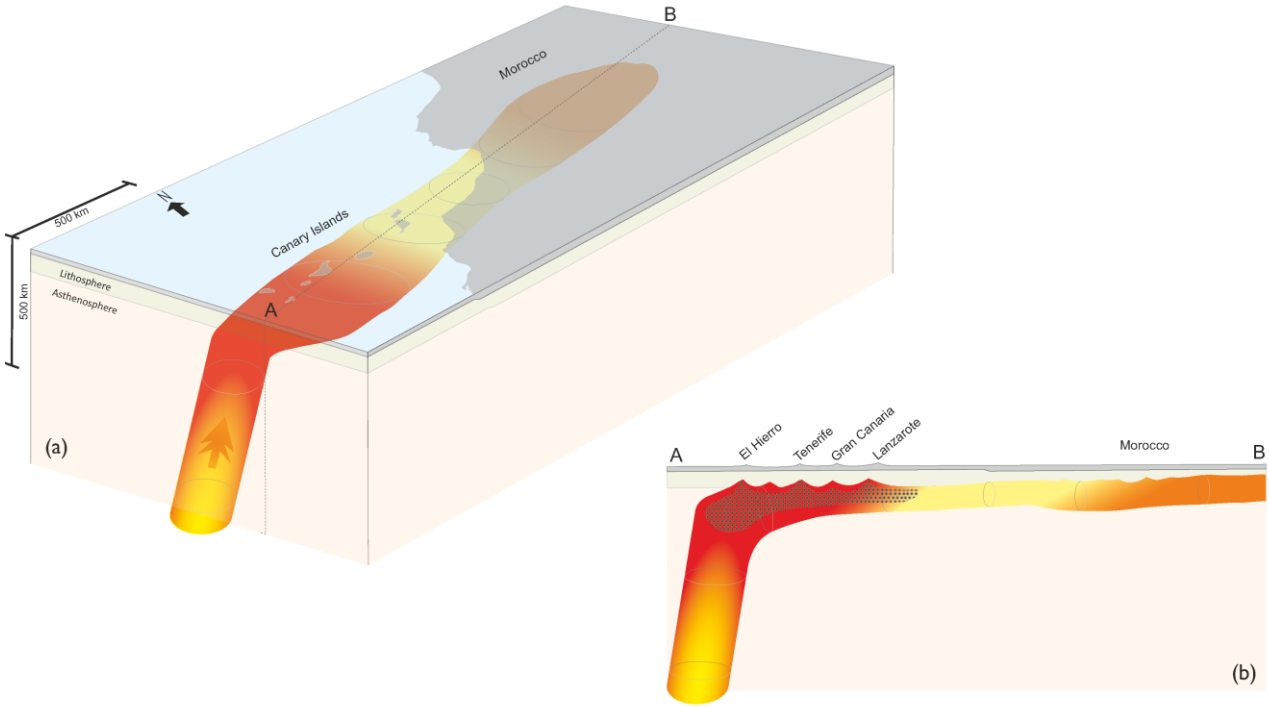

Upwelling plumes are likely to rise significantly faster than the ambient mantle flow (Steinberger and Antretter, 2006), with conduit velocity decreasing radially out from the centreline. The exact velocity profile within the conduit is uncertain, and can be formulated to be a function of temperature and viscosity profile across the plume conduit (Hauri et al., 1994; Olson et al., 1993; Watson and McKenzie, 1991). A result of such a pipe-flow velocity profile would be that an initially planar interface between two mantle heterogeneities would stretch out to form a dome or pinnacle with ascent through the plume. As the pinnacle enters the melt zone, this would yield magmas that comprise components of material above and below the interface (Fig. 8(b)). An effect of a vertically elongate interface would be to prolong

the transition to an incoming heterogeneity, or in the case of a fixed transition time (0.3 Myr), it would require a plume ascent rate proportionally faster than 167 km.Myr^{-1}. If the velocity at 0.7r from the axis is ~10 times slower than at the centreline (Farnetani and Hofmann, 2009) a rise from 700 km depth would result in >500 km of relief on the boundary, requiring either high-velocity ascent or a protracted transition period.

An exponentially declining radial velocity profile is likely to result in different strain rates across the plume stem. In the course of ascent through the whole mantle, this could modify a planar heterogeneity into elongate, roughly axis-parallel, filament-like forms. For example, a 10 km diameter heterogeneity could be stretched vertically to ~300 km during a 700 km rise (Farnetani and Hofmann, 2009). Hence such differential strain produces dispersion and interdigitation of heterogeneities at a given height in the plume as shown in Fig. 8(c). Passage of these vertically stretched and convoluted boundaries through the melt zone would again result in a prolonged transition between heterogeneities or an unrealistically fast ascent rate at a fixed transition. In the case of larger heterogeneities, say 200-500 km blocks, which greatly exceed the diameter of the plume stem, then their boundaries would become similarly stretched and convoluted. However, beneath the convoluted boundary region, the "core" of the heterogeneity could remain isolated and relatively pure during ascent (Farnetani et al., 2012), resulting in periods of prolonged isotopic consistency.

Viscosity and velocity will decline outwards from the plume axis in response to temperature decreasing to that of the ambient mantle. However, plume heterogeneities may reflect different metasomatic origins and petrological types, such as peridotite, eclogite and pyroxenite (Gurenko et al., 2009; Sobolev et al., 2007), generating contrasting viscosities at essentially the same temperature. Farnetani et al. (2018) considered such rheological heterogeneities within a plume dynamic model. Critically, they found that if a heterogeneity had a viscosity >10 times that of the surrounding plume material it was likely to retain its initial form without significant stretching or deformation during ascent (Fig. 8(d)). If such mantle "blobs" with a contrasting rheology to their host also are isotopically distinct, then their passage through the melt zone would be observed in the volcanic output.

Of the plume structures presented in Fig. 8, the radially constant velocity and viscosity model (Fig. 8(a)) would produce the observed temporal isotopic changes. However, most calculated plume dynamic models conflict with this in that they require a progressive outward decline in velocity as depicted in Fig. 8 (b) and (c). Such a velocity gradient is predicted to create a strong vertical re-distribution and dispersion of material in the stem. This would essentially prevent both the abrupt isotopic changes and the persistent isotope ratios such as

those recorded by Canary volcanism. If the heterogeneities have a greater viscosity than the matrix, as represented in Fig. 8(d), there is the potential for a hybrid model which satisfies the requirement for variable physical properties and could produce the observed systematic isotopic pattern.

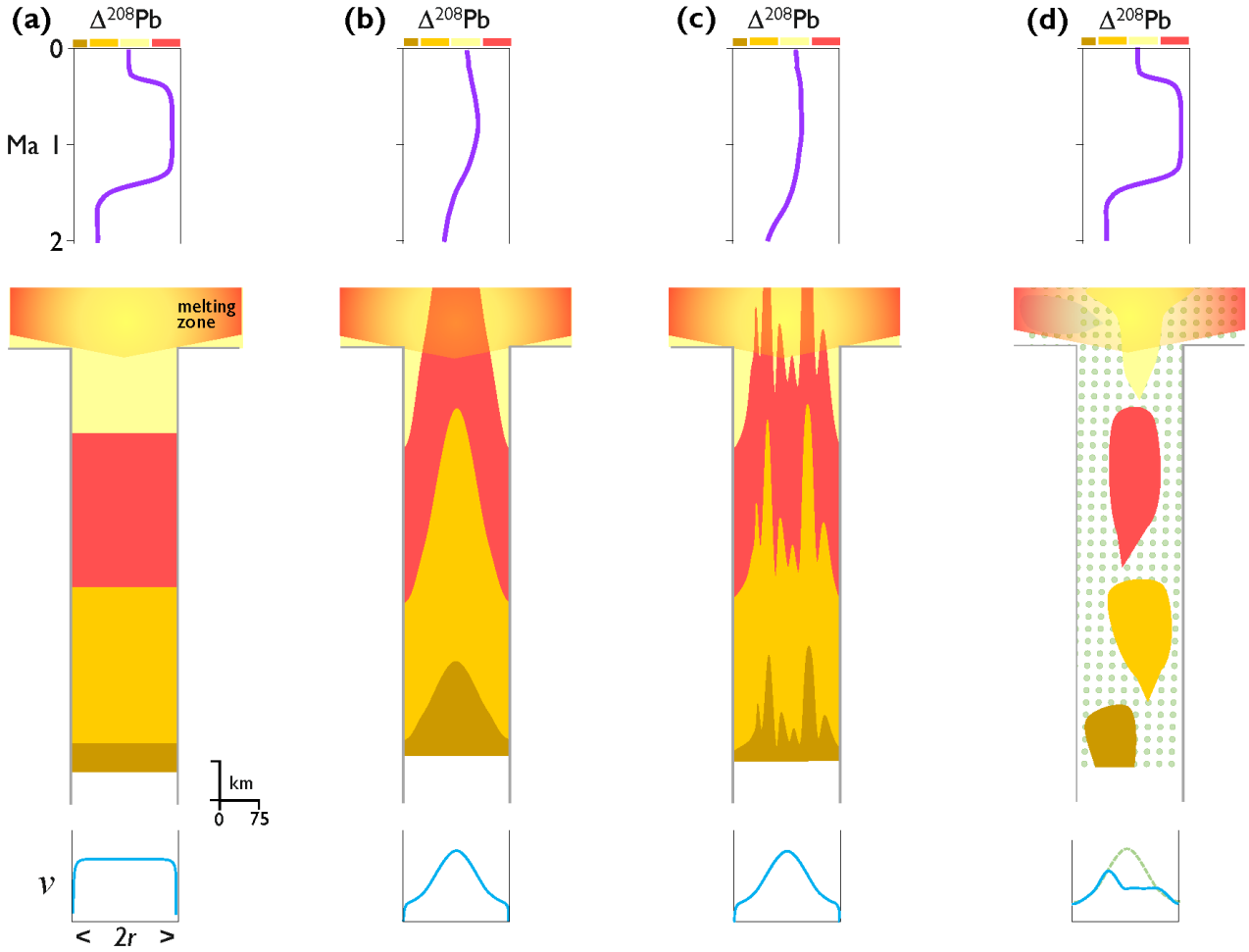

Fig. 8 *Schematic showing the isotopic variation of magmatism in response to heterogeneity distribution and mantle dynamic models. Colours within the plume stem represent regions of mantle with different* $\Delta^{208}Pb/^{204}Pb$*. Plot below each plume shows the model's velocity (v) profile across the plume diameter (2r). Plot above each plume shows the expected temporal changes in* $\Delta^{208}Pb/^{204}Pb$ *with the passage of heterogeneities through a 50 km thick melting zone.* ***(a)*** *Assumes heterogeneities exist as discrete cylinders within the plume stem with a rapid decrease in velocity at the plume margin (e.g. (Blichert-Toft et al., 2003)). Plume upwelling rate calculated as ~167 km* Myr^{-1} *based on the observed 0.3 Myr transition of heterogeneity boundaries through a 50 km melting interval;* ***(b)*** *velocity of the plume declining radially outwards with decreasing temperature and increasing viscosity (e.g. (Hauri et al., 1994; Olson et al., 1993; Watson and McKenzie, 1991)). This schematic assumes plume centreline velocity is ~300 km* Myr^{-1} *and is 150 km* Myr^{-1} *at 0.9*r from axis, with a total rise of 650 km.* ***(c)*** *As for model in (b) except boundaries between heterogeneities are stretched and convoluted in response to high strain rates – particularly at 0.5*r from centreline (Farnetani and Hofmann, 2009).* ***(d)*** *Heterogeneities exist as discrete blobs of higher viscosity material within a lower*

viscosity peridotitic matrix (green dots). Blobs depicted are 10 times more viscous than the matrix (λ = 10) and start ascent as a sphere (Farnetani et al., 2018). Dashed velocity profile shows matrix ascent, solid line shows a representative profile intersecting a heterogeneity.

In order to dominate the signature of the output, these heterogeneities must fill a significant proportion of the melt generation zone, so should be >30 km in diameter (Fig. 8(d)), but presumably less than the diameter of the plume stem (150 km ± 50). Potentially the heterogeneities could be smaller, and more numerous, but for this to be the case they would need to be of equivalent isotopic composition across a given level in the plume to produce the definitive temporal changes. If their size is reduced, the situation will approach the pipe-flow model, with initially adjacent heterogeneities becoming scattered vertically by the radially declining velocity of the matrix, resulting in a pattern similar to Fig. 8(c).

With the transition to an incoming isotopic signature taking 0.3 Myr, the heterogeneity should have a similar nominal ascent rate of ~167 km.Myr^{-1} to the cylinder model. Adding the 1 Myr duration of a heterogeneity to the incoming period provides an estimate of ~217 km for its vertical scale. This equates to a 40 km radius sphere deforming to a cylinder of 34 km radius by 217 km height resulting in a 2.7 times increase in surface area. In terms of a viscosity contrast, these dimensions correspond to the heterogeneity having a 6 times greater viscosity than that of the matrix (λ ~6; Farnetani et al. (2018)).

The isotope composition of the matrix must also contribute to the volcanic output. If the matrix is depleted peridotite, with potentially lower Pb content relative to the heterogeneities, then it would have a reduced contribution to the isotopic inventory. However, it is plausible that an effect of increasing the proportion of matrix in the melt generation zone is to shift compositions along Δ-trajectories toward low $^{206}Pb/^{204}Pb$ or vice-versa.

The differing scales and relationships between these isotopic heterogeneities provide information on how they developed. Variation in mantle κ generates a proportionally greater spread in $^{206}Pb/^{204}Pb$ relative to $^{208}Pb/^{204}Pb$ (dashed line in Figure 5) and creates the shallow alignments in $^{206}Pb/^{204}Pb$-$^{208}Pb/^{204}Pb$ observed in Hawaii, the Azores, Cape Verde and Iceland (Abouchami et al., 2005; Barker et al., 2010; Peate et al., 2010). This relationship is compatible with U-enriched altered ocean crust that is subsequently variably dehydrated during subduction by removal of Pb>U>Th (Kelley et al., 2005; Stracke et al., 2003). Our estimates suggest that 500-800 km domains with broadly similar κ exist within the plume source.

Within these large-scale κ-heterogeneities, Δ-trajectories represent mantle with consistent κ and should exist on original diameter scales of ~30-100 km. We speculate that this is a relic of ocean crust segmentation or domains of subduction dehydration feeding arcs. Displacement along the Δ-trajectories is a function of variable μ and ω (where $\mu \propto \omega$) which equates to a re-distribution of U and Th relative to Pb within, and possibly across the Δ-trajectories.□ Potentially this variation could relate to the proportions of depleted peridotite matrix, which may be derived from intrinsic subducted sub-oceanic lithospheric mantle. Alternatively, it could reflect melt metasomatism (e.g. Pilet et al. (2008)) in which carbonated melts remove, transport and locally concentrate U and Th through chemical reactions.

7. Conclusions

Using high-resolution Pb isotopes, we have investigated temporal changes in output from a mantle plume. A detailed examination of the most recent 2 Myr of volcanism on Tenerife, indicates that the isotopic composition of felsic and basaltic magmas changed synchronously in response to chemical pulses transiting through the plume stem into the plume head. Basaltic volcanics are observed to switch between trajectories with high and low $\Delta^{208}Pb/^{204}Pb$ over periods of ~0.3 Myr, while retaining a $\Delta^{208}Pb/^{204}Pb$ signature for ~1 Myr. Through the course of 11 Myr on Tenerife, six such ~1 Myr $\Delta^{208}Pb/^{204}Pb$ trajectories are identified. Expanding this to the other Canary volcanic centres it is noted that broad changes in $\Delta^{208}Pb/^{204}Pb$ over ~ 4 Myr periods are roughly synchronous and progressive across the plume head. This is consistent with the plume outflow delivering heterogeneities rapidly beneath the lithosphere.

The ascent rate of heterogeneities in the plume is estimated from the 0.3 Myr transition between $\Delta^{208}Pb/^{204}Pb$ trajectories as ~167 km Myr^{-1}, which is of a similar order to an estimate of the outflow velocity across the plume head. Based on the duration and influence of the $\Delta^{208}Pb/^{204}Pb$ fluctuations the ~1 Myr pulses mark the ascent of discrete parcels of mantle ~100-200 km high and 30-100 km diameter. On longer timescales of ~4 Myr, progressive changes indicate these pulses form part of 500-800 km domains extending through the plume column. These indications of the size of chemical heterogeneities in a plume provide a guide to the scale of recycled crustal material with a common origin residing in the deep mantle.

References:

Ablay, G.J., Ernst, G.G.J., Marti, J., Sparks, R.S.J., 1995. THE ~2 Ka subplinian eruption of Montana-Blanca, Tenerife. Bulletin of Volcanology 57, 337-355.

Abouchami, W., Hofmann, A.W., Galer, S.J.G., Frey, F.A., Eisele, J., Feigenson, M., 2005. Lead isotopes reveal bilateral asymmetry and vertical continuity in the Hawaiian mantle plume. Nature 434, 851-856.

Ancochea, E., Fuster, J.M., Ibarrola, E., Cendrero, A., Coello, J., Hernan, F., Cantagrel, J.M., Jamond, C., 1990. Volcanic evolution of the island of Tenerife (Canary Islands in the light of new K-Ar data. Journal of Volcanology and Geothermal Research 44, 231-249.

Ballmer, M.D., Ito, G., van Hunen, J., Tackley, P.J., 2011. Spatial and temporal variability in Hawaiian hotspot volcanism induced by small-scale convection. Nature Geoscience 4, 457-460.

Ballmer, M.D., Ito, G., Wolfe, C.J., Solomon, S.C., 2013. Double layering of a thermochemical plume in the upper mantle beneath Hawaii. Earth and Planetary Science Letters 376, 155-164.

Barker, A.K., Holm, P.M., Peate, D.W., Baker, J.A., 2010. A 5 million year record of compositional variations in mantle sources to magmatism on Santiago, southern Cape Verde archipelago. Contributions to Mineralogy and Petrology 160, 133-154.

Beier, C., Haase, K.M., Abouchami, W., Krienitz, M.S., Hauff, F., 2008. Magma genesis by rifting of oceanic lithosphere above anomalous mantle: Terceira Rift, Azores. Geochemistry Geophysics Geosystems 9.

Blichert-Toft, J., Weis, D., Maerschalk, C., Agranier, A., Albarède, F., 2003. Hawaiian hot spot dynamics as inferred from the Hf and Pb isotope evolution of Mauna Kea volcano. Geochemistry, Geophysics, Geosystems 4.

Bonnin, M., Nolet, G., Villaseñor, A., Gallart, J., Thomas, C., 2014. Multiple-frequency tomography of the upper mantle beneath the African/Iberian collision zone. Geophysical Journal International 198, 1458-1473.

Bourdon, B., Ribe, N.M., Stracke, A., Saal, A.E., Turner, S.P., 2006. Insights into the dynamics of mantle plumes from uranium-series geochemistry. Nature 444, 713-717.

Brown, R.J., Barry, T.L., Branney, M.J., Pringle, M.S., Bryan, S.E., 2003. The Quaternary pyroclastic succession of southeast Tenerife, Canary Islands: explosive eruptions, related caldera subsidence, and sector collapse. Geological Magazine 140, 265-288.

Carracedo, J.C., Guillou, H., Nomade, S., Rodriguez-Badiola, E., Perez-Torrado, F.J., Rodriguez-Gonzalez, A., Paris, R., Troll, V.R., Wiesmaier, S., Delcamp, A., Fernandez-Turiel,

J.L., 2011. Evolution of ocean-island rifts: The northeast rift zone of Tenerife, Canary Islands. Geological Society of America Bulletin 123, 562-584.
Carracedo, J.C., Rodriguez Badiola, E., Guillou, H., Paterne, M., Scaillet, S., Perez Torrado, F.J., Paris, R., Fra-Paleo, U., Hansen, A., 2007. Eruptive and structural history of Teide Volcano and rift zones of Tenerife, Canary Islands. Geological Society of America Bulletin 119, 1027-1051.
Chauvel, C., Maury, R.C., Blais, S., Lewin, E., Guillou, H., Guille, G., Rossi, P., Gutscher, M.-A., 2012. The size of plume heterogeneities constrained by Marquesas isotopic stripes. Geochemistry, Geophysics, Geosystems 13.
Cousens, B.L., Spera, F.J., Tilton, G.R., 1990. Isotopic patterns in silicic ignimbrites and lava flows of the Mogan and lower Fataga Formations, Gran Canaria, Canary Islands: temporal changes in mantle source composition. Earth and Planetary Science Letters 96, 319-335.
Davila-Harris, P., Ellis, B.S., Branney, M.J., Carrasco-Nunez, G., 2013. Lithostratigraphic analysis and geochemistry of a vitric spatter-bearing ignimbrite: the Quaternary Adeje Formation, Canadas volcano, Tenerife. Bulletin of Volcanology 75.
Dávila Harris, P., 2009. Explosive ocean-island volcanism: The 1.8–0.7 Ma explosive eruption history of Cañadas volcano recorded by the pyroclastic successions around Adeje and Abona, southern Tenerife, Canary Islands. PhD thesis. University of Leicester, Leicester, p. 311.
Deegan, F.M., Troll, V.R., Barker, A.K., Harris, C., Chadwick, J.P., Carracedo, J.C., Delcamp, A., 2012. Crustal versus source processes recorded in dykes from the Northeast volcanic rift zone of Tenerife, Canary Islands. Chemical Geology 334, 324-344.
Duggen, S., Hoernle, K.A., Hauff, F., Klügel, A., Bouabdellah, M., Thirlwall, M.F., 2009. Flow of Canary mantle plume material through a subcontinental lithospheric corridor beneath Africa to the Mediterranean. Geology 37, 283-286.
Edgar, C.J., Wolff, J.A., Olin, P.H., Nichols, H.J., Pittari, A., Cas, R.A.F., Reiners, P.W., Spell, T.L., Martí, J., 2007. The late Quaternary Diego Hernandez Formation, Tenerife: Volcanology of a complex cycle of voluminous explosive phonolitic eruptions. Journal of Volcanology and Geothermal Research 160, 59-85.
Elliott, T., Zindler, A., Bourdon, B., 1999. Exploring the kappa conundrum: the role of recycling in the lead isotope evolution of the mantle. Earth and Planetary Science Letters 169, 129-145.
Farnetani, C.G., Hofmann, A.W., 2009. Dynamics and internal structure of a lower mantle plume conduit. Earth and Planetary Science Letters 282, 314-322.

Farnetani, C.G., Hofmann, A.W., 2010. Dynamics and internal structure of the Hawaiian plume. Earth and Planetary Science Letters 295, 231-240.
Farnetani, C.G., Hofmann, A.W., Class, C., 2012. How double volcanic chains sample geochemical anomalies from the lowermost mantle. Earth and Planetary Science Letters 359-360, 240-247.
Farnetani, C.G., Hofmann, A.W., Duvernay, T., Limare, A., 2018. Dynamics of rheological heterogeneities in mantle plumes. Earth and Planetary Science Letters 499, 74-82.
Fontaine, F.R., Barruol, G., Tkalčić, H., Wölbern, I., Rümpker, G., Bodin, T., Haugmard, M., 2015. Crustal and uppermost mantle structure variation beneath La Réunion hotspot track. Geophysical Journal International 203, 107-126.
Fuster, J.M., Ibarrola, E., Snelling, N.J., Cantagrel, J.M., Huertas, M.J., Coello, J., Ancochea, E., 1994. Cronologıa K–Ar de la Formacion Canadas en el sector suroeste de Tenerife: implicaciones de los episodios piroclasticos en la evolucion volcanica. Boletin Real Sociedad Espanola de Historia Natural - Seccion Geologica 89, 25-41.
Gale, A., Dalton, C.A., Langmuir, C.H., Su, Y.J., Schilling, J.G., 2013. The mean composition of ocean ridge basalts. Geochemistry Geophysics Geosystems 14, 489-518.
Geldmacher, J., Hoernle, K., van der Bogaard, P., Duggen, S., Werner, R., 2005. New Ar-40/Ar-39 age and geochemical data from seamounts in the Canary and Madeira volcanic provinces: Support for the mantle plume hypothesis. Earth and Planetary Science Letters 237, 85-101.
Genske, F.S., Beier, C., Stracke, A., Turner, S.P., Pearson, N.J., Hauff, F., Schaefer, B.F., Haase, K.M., 2016. Comparing the nature of the western and eastern Azores mantle. Geochimica et Cosmochimica Acta 172, 76-92.
Gibson, S.A., Geist, D.J., Richards, M.A., 2015. Mantle plume capture, anchoring, and outflow during Galápagos plume-ridge interaction. Geochemistry, Geophysics, Geosystems 16, 1634-1655.
Guillou, H., Carracedo, J.C., Paris, R., Torrado, F.J.P., 2004. Implications for the early shield-stage evolution of Tenerife from K/Ar ages and magnetic stratigraphy. Earth and Planetary Science Letters 222, 599-614.
Gurenko, A.A., Hoernle, K.A., Hauff, F., Schmincke, H.U., Han, D., Miura, Y.N., Kaneoka, I., 2006. Major, trace element and Nd-Sr-Pb-O-He-Ar isotope signatures of shield stage lavas from the central and western Canary Islands: Insights into mantle and crustal processes. Chemical Geology 233, 75-112.

Gurenko, A.A., Sobolev, A.V., Hoernle, K.A., Hauff, F., Schmincke, H.-U., 2009. Enriched, HIMU-type peridotite and depleted recycled pyroxenite in the Canary plume: A mixed-up mantle. Earth and Planetary Science Letters 277, 514-524.

Hauri, E.H., Whitehead, J.A., Hart, S.R., 1994. Fluid Dynamic and Geochemical Aspects of Entrainment in Mantle Plumes. Journal of Geophysical Research-Solid Earth 99, 24275-24300.

Hoernle, K., Schmincke, H.U., 1993. The role of partial melting in the 15 Ma geochemical evolution of Gran Canaria - a blob model for the Canary hotspot. Journal of Petrology 34, 599-626.

Hoernle, K., Tilton, G., Schmincke, H.U., 1991. Sr-Nd-Pb isotopic evolution of Gran-Canaria - evidence for shallow enriched mantle beneath the Canary Islands. Earth and Planetary Science Letters 106, 44-63.

Huang, S., Hall, P.S., Jackson, M.G., 2011. Geochemical zoning of volcanic chains associated with Pacific hotspots. Nature Geosci 4, 874-878.

Huertas, M.J., Arnaud, N.O., Ancochea, E., Cantagrel, J.M., Fuster, J.M., 2002. Ar-40/Ar-39 stratigraphy of pyroclastic units from the Canadas Volcanic Edifice (Tenerife, Canary Islands) and their bearing on the structural evolution. Journal of Volcanology and Geothermal Research 115, 351-365.

Ito, G., Mahoney, J.J., 2005. Flow and melting of a heterogeneous mantle: 1. Method and importance to the geochemistry of ocean island and mid-ocean ridge basalts. Earth and Planetary Science Letters 230, 29-46.

Jackson, M.G., Hart, S.R., Konter, J.G., Kurz, M.D., Blusztajn, J., Farley, K.A., 2014. Helium and lead isotopes reveal the geochemical geometry of the Samoan plume. Nature 514, 355-358.

Jackson, M.G., Weis, D., Huang, S., 2012. Major element variations in Hawaiian shield lavas: Source features and perspectives from global ocean island basalt (OIB) systematics. Geochemistry, Geophysics, Geosystems 13, Q09009.

Jones, T.D., Davies, D.R., Campbell, I.H., Iaffaldano, G., Yaxley, G., Kramer, S.C., Wilson, C.R., 2017. The concurrent emergence and causes of double volcanic hotspot tracks on the Pacific plate. Nature 545, 472-476.

Kelley, K.A., Plank, T., Farr, L., Ludden, J., Staudigel, H., 2005. Subduction cycling of U, Th, and Pb. Earth and Planetary Science Letters 234, 369-383.

Kitagawa, H., Kobayashi, K., Makishima, A., Nakamura, E., 2008. Multiple Pulses of the Mantle Plume: Evidence from Tertiary Icelandic Lavas. Journal of Petrology 49, 1365-1396.

Marske, J.P., Pietruszka, A.J., Weis, D., Garcia, M.O., Rhodes, J.M., 2007. Rapid passage of a small-scale mantle heterogeneity through the melting regions of Kilauea and Mauna Loa Volcanoes. Earth and Planetary Science Letters 259, 34-50.

Martinez-Arevalo, C., Mancilla, F.d.L., Helffrich, G., Garcia, A., 2013. Seismic evidence of a regional sublithospheric low velocity layer beneath the Canary Islands. Tectonophysics 608, 586-599.

Massmeyer, A., Di Giuseppe, E., Davaille, A., Rolf, T., Tackley, P.J., 2013. Numerical simulation of thermal plumes in a Herschel–Bulkley fluid. Journal of Non-Newtonian Fluid Mechanics 195, 32-45.

Mériaux, C.A., Duarte, J.C., Duarte, S.S., Schellart, W.P., Chen, Z., Rosas, F., Mata, J., Terrinha, P., 2015. Capture of the Canary mantle plume material by the Gibraltar arc mantle wedge during slab rollback. Geophysical Journal International 201, 1717-1721.

Miller, M.S., O'Driscoll, L.J., Butcher, A.J., Thomas, C., 2015. Imaging Canary Island hotspot material beneath the lithosphere of Morocco and southern Spain. Earth and Planetary Science Letters 431, 186-194.

Olson, P., Schubert, G., Anderson, C., 1993. Structure of axisymmetric mantle plumes. Journal of Geophysical Research: Solid Earth 98, 6829-6844.

Parnell-Turner, R., White, N., Henstock, T., Murton, B., Maclennan, J., Jones, S.M., 2014. A continuous 55-million-year record of transient mantle plume activity beneath Iceland. Nature Geoscience 7, 914.

Peate, D.W., Breddam, K., Baker, J.A., Kurz, M.D., Barker, A.K., Prestvik, T., Grassineau, N., Skovgaard, A.C., 2010. Compositional Characteristics and Spatial Distribution of Enriched Icelandic Mantle Components. Journal of Petrology 51, 1447-1475.

Pilet, S., Baker, M.B., Stolper, E.M., 2008. Metasomatized lithosphere and the origin of alkaline lavas. Science 320, 916-919.

Ren, Z.-Y., Ingle, S., Takahashi, E., Hirano, N., Hirata, T., 2005. The chemical structure of the Hawaiian mantle plume. Nature 436, 837.

Rudge, J.F., Maclennan, J., Stracke, A., 2013. The geochemical consequences of mixing melts from a heterogeneous mantle. Geochimica et Cosmochimica Acta 114, 112-143.

Rychert, C.A., Harmon, N., Ebinger, C., 2014. Receiver function imaging of lithospheric structure and the onset of melting beneath the Galapagos Archipelago. Earth and Planetary Science Letters 388, 156-165.

Rychert, C.A., Laske, G., Harmon, N., Shearer, P.M., 2013. Seismic imaging of melt in a displaced Hawaiian plume. Nature Geoscience 6, 657-660.

Shorttle, O., Maclennan, J., Piotrowski, A.M., 2013. Geochemical provincialism in the Iceland plume. Geochimica Et Cosmochimica Acta 122, 363-397.
Simonsen, S.L., Neumann, E.R., Seim, K., 2000. Sr-Nd-Pb isotope and trace-element geochemistry evidence for a young HIMU source and assimilation at Tenerife (Canary Island). Journal of Volcanology and Geothermal Research 103, 299-312.
Sims, K.W.W., DePaolo, D.J., Murrell, M.T., Baldridge, W.S., Goldstein, S., Clague, D., Jull, M., 1999. Porosity of the melting zone and variations in the solid mantle upwelling rate beneath Hawaii: inferences from 238U-230Th-226Ra and 235U-231Pa disequilibria. Geochimica et Cosmochimica Acta 63, 4119-4138.
Sims, K.W.W., Maclennan, J., Blichert-Toft, J., Mervine, E.M., Blusztajn, J., Grönvold, K., 2013. Short length scale mantle heterogeneity beneath Iceland probed by glacial modulation of melting. Earth and Planetary Science Letters 379, 146-157.
Sliwinski, J.T., Bachmann, O., Ellis, B.S., Davila-Harris, P., Dufek, J., 2015. Eruption of Shallow Crystal Cumulates during Explosive Phonolitic Eruptions on Tenerife, Canary Islands. Journal of Petrology 56, 2173-2194.
Sobolev, A.V., Hofmann, A.W., Kuzmin, D.V., Yaxley, G.M., Arndt, N.T., Chung, S.-L., Danyushevsky, L.V., Elliott, T., Frey, F.A., Garcia, M.O., Gurenko, A.A., Kamenetsky, V.S., Kerr, A.C., Krivolutskaya, N.A., Matvienkov, V.V., Nikogosian, I.K., Rocholl, A., Sigurdsson, I.A., Sushchevskaya, N.M., Teklay, M., 2007. The Amount of Recycled Crust in Sources of Mantle-Derived Melts. Science 316, 412-417.
Steinberger, B., Antretter, M., 2006. Conduit diameter and buoyant rising speed of mantle plumes: Implications for the motion of hot spots and shape of plume conduits. Geochemistry Geophysics Geosystems 7.
Stock, M.J., Taylor, R.N., Gernon, T.M., 2012. Triggering of major eruptions recorded by actively forming cumulates. Scientific Reports 2.
Stracke, A., Bizimis, M., Salters, V.J.M., 2003. Recycling oceanic crust: Quantitative constraints. Geochemistry Geophysics Geosystems 4.
Stracke, A., Bourdon, B., McKenzie, D., 2006. Melt extraction in the Earth's mantle: Constraints from U–Th–Pa–Ra studies in oceanic basalts. Earth and Planetary Science Letters 244, 97-112.
Taylor, R.N., Ishizuka, O., Michalik, A., Milton, J.A., Croudace, I.W., 2015. Evaluating the precision of Pb isotope measurement by mass spectrometry. Journal of Analytical Atomic Spectrometry 30, 198-213.
Thirlwall, M.F., 1997. Pb isotopic and elemental evidence for OIB derivation from young HIMU mantle. Chemical Geology 139, 51-74.

Thirlwall, M.F., Singer, B.S., Marriner, G.F., 2000. Ar-39-Ar-40 ages and geochemistry of the basaltic shield stage of Tenerife, Canary Islands, Spain. Journal of Volcanology and Geothermal Research 103, 247-297.

Turner, S., Kokfelt, T., Hoernle, K., Johansen, T.S., Hauff, F., Lundstrom, C., van den Bogaard, P., Klügel, A., 2017. Contrasting magmatic cannibalism forms evolved phonolitic magmas in the Canary Islands. Geology 45, 147-150.

Watson, S., McKenzie, D.A.N., 1991. Melt Generation by Plumes: A Study of Hawaiian Volcanism. Journal of Petrology 32, 501-537.

Wiesmaier, S., Troll, V.R., Carracedo, J.C., Ellam, R.M., Bindeman, I., Wolff, J.A., 2012. Bimodality of Lavas in the Teide-Pico Viejo Succession in Tenerife-the Role of Crustal Melting in the Origin of Recent Phonolites. Journal of Petrology 53, 2465-2495.

Workman, R.K., Hart, S.R., 2005. Major and trace element composition of the depleted MORB mantle (DMM). Earth and Planetary Science Letters 231, 53-72.

Table 1. Pb isotopes of Tenerife felsic volcanics and syenites. Age references (Ablay et al., 1995; Ancochea et al., 1990; Brown et al., 2003; Dávila Harris, 2009; Edgar et al., 2007; Huertas et al., 2002)

location/unit	sample	lithology	UTM long	UTM lat	$^{206}Pb/^{204}Pb$	$^{207}Pb/^{204}Pb$	$^{208}Pb/^{204}Pb$	207*/206*	208*/206*	208*t/206*t	Δ7/4	Δ8/4	age Ma.	age reference
felsic volcanics < 2 Ma														
Montana Blanca	TF30	**obsidian**	28R 342545E	3128177N	**19.7773**	**15.6180**	**39.5870**	0.50820	0.96577	1.0289	**-1.7**	**4.9**	0.002	Ablay et al., 1995
	TF75	**pumice**	28R 342803E	3127274N	**19.7737**	**15.6159**	**39.5785**	0.50818	0.96529	1.0278	**-1.9**	**4.5**	0.002	
	TF31†	**obsidian**	28R 342376E	3128619N	**19.7783**	**15.6192**	**39.5776**	0.50826	0.96479	1.0264	**-1.6**	**3.9**	0.002	
	TF394	**phonolite**	28R 342326E	3126997N	**19.7775**	**15.6173**	**39.5852**	0.50812	0.96559	1.0284	**-1.8**	**4.7**	0.002	
Abrigo - juvenile	TF206(y)	**pumice**	28R 359969E	3120540N	**19.7766**	**15.6191**	**39.5700**	0.50834	0.96422	1.0251	**-1.6**	**3.3**	0.17	Brown et al., 2003
	TF206(z)	**pumice**	28R 359969E	3120540N	**19.7790**	**15.6195**	**39.5844**	0.50826	0.96537	1.0279	**-1.6**	**4.5**	0.17	
La Caleta	TF101-LC1	**pumice**	28R 358221E	3118883N	**19.7941**	**15.6164**	**39.6060**	0.50723	0.96604	1.0293	**-2.0**	**4.8**	0.22	Brown et al., 2003
	TF101-LC2	**pumice**	28R 358221E	3118883N	**19.7968**	**15.6164**	**39.6092**	0.50711	0.96610	1.0294	**-2.1**	**4.8**	0.22	
	TF101-LC3	**pumice**	28R 358221E	3118883N	**19.7975**	**15.6159**	**39.6059**	0.50703	0.96573	1.0285	**-2.1**	**4.4**	0.22	
	TF101-LC4	**pumice**	28R 358221E	3118883N	**19.8026**	**15.6190**	**39.6167**	0.50707	0.96628	1.0298	**-1.9**	**4.8**	0.22	
	TF101-LC5	**pumice**	28R 358221E	3118883N	**19.7987**	**15.6198**	**39.6168**	0.50733	0.96665	1.0307	**-1.7**	**5.3**	0.22	
Poris	TF96-P1	**pumice**	28R 358221E	3118883N	**19.8011**	**15.6197**	**39.6237**	0.50721	0.96709	1.0318	**-1.8**	**5.7**	0.27	Brown et al., 2003
	TF101-P2	**pumice**	28R 355764E	3110404N	**19.8035**	**15.6179**	**39.6221**	0.50692	0.96671	1.0308	**-2.0**	**5.3**	0.27	
	TF101-P3	**pumice**	28R 355764E	3110404N	**19.8023**	**15.6184**	**39.6221**	0.50703	0.96683	1.0311	**-1.9**	**5.4**	0.27	
Fasnia	TF201-F1	**pumice**	28R 358151E	3118852N	**19.7836**	**15.6162**	**39.6067**	0.50772	0.96708	1.0320	**-1.9**	**6.1**	0.29	
	TF137-F2	**pumice**	28R 357961E	3118928N	**19.7838**	**15.6149**	**39.6033**	0.50759	0.96674	1.0312	**-2.1**	**5.8**	0.29	Brown et al., 2003 &
	TF137-F4(c)	**pumice**	28R 357961E	3118928N	**19.7853**	**15.6140**	**39.6035**	0.50743	0.96661	1.0309	**-2.2**	**5.6**	0.29	Edgar et al., 2007
	TF137-F3	**pumice**	28R 357961E	3118928N	**19.7845**	**15.6149**	**39.6053**	0.50755	0.96686	1.0315	**-2.1**	**5.9**	0.29	
La Tarta	TF-LT1	**pumice**	28R 353952E	3135097N	**19.7810**	**15.6182**	**39.6072**	0.50804	0.96738	1.0328	**-1.7**	**6.5**	*0.32*	Brown et al., 2003
	TF-LT2	**pumice**	28R 353952E	3135097N	**19.7927**	**15.6194**	**39.6223**	0.50759	0.96773	1.0335	**-1.7**	**6.6**	*0.32*	
Fortaleza	TF-FL1	**phonolite**	28R 343830E	3133032N	**19.7732**	**15.6186**	**39.6113**	0.50846	0.96847	1.0356	**-1.6**	**7.8**	0.37	Anochea et al., 1990
	TF-FL2	**phonolite**	28R 343830E	3133032N	**19.7697**	**15.6149**	**39.6109**	0.50828	0.96877	1.0364	**-1.9**	**8.2**	0.37	
Granadilla	TF211(a)	**pumice**	28R 348750E	3111141N	**19.7470**	**15.6126**	**39.6099**	0.50916	0.97077	1.0418	**-1.9**	**10.9**	0.60	Brown et al., 2003
	TF211(b)	**pumice**	28R 348750E	3111141N	**19.7568**	**15.6148**	**39.6238**	0.50889	0.97119	1.0427	**-1.8**	**11.1**	0.60	
	TF211(a)	**pumice leach 1**	28R 348750E	3111141N	**19.7433**	**15.6145**	**39.6102**	0.50952	0.97115	1.0428	**-1.7**	**11.4**	0.60	
	TF211(a)	**pumice leach 2**	28R 348750E	3111141N	**19.7510**	**15.6146**	**39.6183**	0.50915	0.97121	1.0428	**-1.7**	**11.2**	0.60	
Abades	TF207(b)	**pumice (black)**	28R 359133E	3115670N	**19.7958**	**15.6216**	**39.6685**	0.50765	0.97184	1.0436	**-1.5**	**10.8**	0.60	Bryan et al., 1998
	TF207(c)	**pumice (dark)**	28R 359133E	3115670N	**19.7911**	**15.6180**	**39.6517**	0.50754	0.97068	1.0408	**-1.8**	**9.7**	0.60	
	TF390	**pumice**	28R 355703E	3110384N	**19.7591**	**15.6175**	**39.6296**	0.50903	0.97153	1.0435	**-1.5**	**11.4**	0.60	
Arico	TF207	**pumice (black)**	28R 359133E	3115670N	**19.7671**	**15.6161**	**39.6251**	0.50851	0.97036	1.0404	**-1.8**	**10.0**	0.67	Brown et al., 2003
	TF207	**pumice (green)**	28R 359133E	3115670N	**19.7638**	**15.6166**	**39.6226**	0.50872	0.97043	1.0406	**-1.7**	**10.1**	0.67	
	TF207	**pumice (dark)**	28R 359133E	3115670N	**19.7694**	**15.6186**	**39.6332**	0.50864	0.97093	1.0418	**-1.5**	**10.5**	0.67	
	TF207	**pumice (non-streaky)**	28R 359133E	3115670N	**19.7571**	**15.6178**	**39.6207**	0.50917	0.97087	1.0419	**-1.5**	**10.7**	0.67	
	TF206	**pumice (green)**	28R 359969E	3120540N	**19.7597**	**15.6154**	**39.6151**	0.50881	0.97010	1.0399	**-1.8**	**9.9**	0.67	
	TF206	**pumice (black)**	28R 359969E	3120540N	**19.7687**	**15.6180**	**39.6287**	0.50862	0.97056	1.0409	**-1.6**	**10.1**	0.67	
	TF208	**pumice**	28R 356615E	3113109N	**19.7664**	**15.6164**	**39.6216**	0.50857	0.97009	1.0398	**-1.7**	**9.7**	0.67	
Helecho	TF361	**phonolite**	28R 350339E	3109921N	**19.7570**	**15.6101**	**39.6115**	0.50843	0.97000	1.0397	**-2.3**	**9.8**	0.733	Davilla-Harris, 2009
Rio	TF357(f)	**pumice**	28R 350423E	3109792N	**19.7344**	**15.6136**	**39.5982**	0.50987	0.97082	1.0421	**-1.7**	**11.2**	0.747	Davilla-Harris, 2009
Tosca	TF320	**pumice**	28R 330146E	3111150N	**19.7392**	**15.6108**	**39.6018**	0.50937	0.97072	1.0418	**-2.0**	**11.0**	0.88	Davilla-Harris, 2009
Guaza	TF349	**phonolite**	28R 333137E	3101195N	**19.7414**	**15.6132**	**39.6120**	0.50949	0.97150	1.0437	**-1.8**	**11.8**	0.93	Davilla-Harris, 2009
Caldera Del Rey	TF323	**phonolite**	28R 330864E	3107778N	**19.7297**	**15.6106**	**39.5920**	0.50982	0.97068	1.0418	**-1.9**	**11.2**	0.953	Davilla-Harris, 2009
Monjas	TF357(e)	**pumice**	28R 350423E	3109792N	**19.6658**	**15.6070**	**39.5249**	0.51261	0.97017	1.0417	**-1.6**	**12.2**	1.310	Davilla-Harris, 2009
	TF357(c)	**pumice**	28R 350423E	3109792N	**19.6636**	**15.6044**	**39.5158**	0.51246	0.96951	1.0400	**-1.8**	**11.5**	1.310	
Mocan	TF357(a)	**pumice**	28R 350423E	3109792N	**19.7234**	**15.6103**	**39.5559**	0.51009	0.96779	1.0347	**-1.9**	**8.3**	1.494	Davilla-Harris, 2009
	TF357(b)	**obsidian**	28R 350423E	3109792N	**19.7247**	**15.6106**	**39.5571**	0.51005	0.96779	1.0347	**-1.9**	**8.3**	1.494	
Vallito	TF359(a)	**pumice**	28R 350144E	3109941N	**19.6855**	**15.6053**	**39.5438**	0.51148	0.97016	1.0413	**-2.0**	**11.7**	*1.50*	Davilla-Harris, 2009
San Juan	TF317a	**obsidian**	28R 323651E	3115990N	**19.6951**	**15.6037**	**39.5527**	0.51085	0.97012	1.0410	**-2.2**	**11.4**	1.500	Davilla-Harris, 2009
	TF317b	**obsidian**	28R 323651E	3115990N	**19.6943**	**15.6031**	**39.5504**	0.51083	0.96997	1.0407	**-2.3**	**11.3**	1.500	
	TF317c	**obsidian**	28R 323651E	3115990N	**19.6942**	**15.6031**	**39.5507**	0.51084	0.97001	1.0408	**-2.3**	**11.3**	1.500	
Barranco del Agua lava	TF316	**phonolite**	28R 330048E	3110809N	**19.7233**	**15.6069**	**39.5637**	0.50976	0.96855	1.0366	**-2.2**	**9.1**	*1.55*	Davilla-Harris, 2009
Adeje	TF315a	**obsidian (plag Φ)**	28R 330048E	3110809N	**19.7044**	**15.6075**	**39.5468**	0.51075	0.96868	1.0373	**-1.9**	**9.7**	1.570	Davilla-Harris, 2009
	TF315b	**obsidian**	28R 330048E	3110809N	**19.7040**	**15.6058**	**39.5405**	0.51061	0.96811	1.0359	**-2.1**	**9.1**	1.570	
	TF315c	**pumice**	28R 330048E	3110809N	**19.7125**	**15.6069**	**39.5488**	0.51029	0.96813	1.0358	**-2.1**	**8.9**	1.570	
Fanabe	TF310a	**pumice**	28R 330408E	3110874N	**19.7221**	**15.6081**	**39.5490**	0.50994	0.96724	1.0334	**-2.1**	**7.8**	1.585	Davilla-Harris, 2009
	TF310b	**pumice**	28R 330408E	3110874N	**19.7230**	**15.6084**	**39.5510**	0.50993	0.96737	1.0337	**-2.1**	**7.9**	1.585	
Barco	TF363	**pumice**	28R 352669E	3111224N	**19.7218**	**15.6102**	**39.5550**	0.51016	0.96785	1.0349	**-1.9**	**8.4**	1.601	Davilla-Harris, 2009
Nicolas	TF313a	**pumice**	28R 330539E	3110870N	**19.7199**	**15.6083**	**39.5485**	0.51007	0.96740	1.0338	**-2.0**	**8.0**	*1.604*	Davilla-Harris, 2009
	TF313b	**pumice**	28R 330539E	3110870N	**19.7174**	**15.6080**	**39.5460**	0.51016	0.96740	1.0339	**-2.0**	**8.1**	*1.604*	
Agua	TF312	**phonolite**	28R 330532E	3110885N	**19.7169**	**15.6074**	**39.5430**	0.51013	0.96716	1.0333	**-2.1**	**7.8**	*1.623*	Davilla-Harris, 2009
	TF314	**phonolite**	28R 330519E	3110882N	**19.7192**	**15.6084**	**39.5487**	0.51011	0.96749	1.0341	**-2.0**	**8.1**	*1.623*	
Enramada	TF321a	**pumice (white)**	28R 328487E	3109266N	**19.7270**	**15.6086**	**39.5497**	0.50975	0.96686	1.0324	**-2.1**	**7.3**	1.661	Davilla-Harris, 2009
	TF321b	**pumice (green)**	28R 328487E	3109266N	**19.7207**	**15.6081**	**39.5454**	0.51001	0.96703	1.0329	**-2.1**	**7.6**	1.661	
	TF321c	**pumice (plag Φ)**	28R 328487E	3109266N	**19.7255**	**15.6086**	**39.5492**	0.50983	0.96696	1.0326	**-2.1**	**7.4**	1.661	
Morteros	TF354(a)	**pumice**	28R 326957E	3110103N	**19.7230**	**15.6102**	**39.5242**	0.51010	0.96479	1.0273	**-1.9**	**5.2**	*1.75*	Davilla-Harris, 2009
Gaviotas	TF355 (c)	**pumice**	28R 326969E	3110132N	**19.7011**	**15.6103**	**39.5167**	0.51119	0.96610	1.0309	**-1.6**	**7.1**	1.84	Huertas et al 2002
	TF216	**pumice**	28R 327006E	3110095N	**19.7221**	**15.6137**	**39.5528**	0.51048	0.96761	1.0343	**-1.5**	**8.2**	1.84	
Syenite - accidental clasts in ignimbrite														
Fasnia	TF-L1-72(a)	**monzonite**	28R 357961E	3118928N	**19.7359**	**15.6121**	**39.5631**	0.50965	0.96732	1.0334	**-1.8**	**7.5**	> 0.29	
Fasnia	TF-L1-72(b)	**syentite**	28R 357961E	3118928N	**19.7611**	**15.6158**	**39.5980**	0.50877	0.96832	1.0355	**-1.7**	**8.0**	> 0.29	Brown et al., 2003
Fasnia	TF-L1-77	**nepheline syenite**	28R 357961E	3118928N	**19.7570**	**15.6156**	**39.5918**	0.50896	0.96811	1.0350	**-1.7**	**7.9**	> 0.29	
San Juan	TR041-01	**Alkali-feldspar syenite**	28R 325923E	3111302N	**19.7109**	**15.6024**	**39.5478**	0.50994	0.96817	1.0359	**-2.5**	**9.0**	> 1.50	Davilla-Harris, 2009
Morteros	TF215(a)	**syenite**	28R 327318E	3110051N	**19.7242**	**15.6158**	**39.5488**	0.51057	0.96704	1.0328	**-1.3**	**7.5**	> 1.75	Davilla-Harris, 2009

* between 0.29Ma and 0.60 Ma

† Pb measured by double spike TIMS

Table 2. Pb isotopes of Tenerife basaltic/mafic volcanics. Samples marked basaltic melt indicate they are interstitial basaltic material separated from mafic cumulate mush nodules from felsic pyroclastics (e.g. Stock et al. (2012)). Age references (Brown et al., 2003; Carracedo et al., 2011; Carracedo et al., 2007; Davila-Harris et al., 2013; Dávila Harris, 2009; Edgar et al., 2007; Fuster et al., 1994; Guillou et al., 2004; Huertas et al., 2002; Thirlwall et al., 2000).

location/unit	sample	lithology	UTM long	UTM lat	$^{206}Pb/^{204}Pb$	$^{207}Pb/^{204}Pb$	$^{208}Pb/^{204}Pb$	207*/206*	208*/206*	208*t/206*t	Δ7/4	Δ8/4	age Ma.	age reference
mafic volcanics < 2 Ma														
Chinyero 1909 AD	TF337	**basanite**	28R 327069E	3130652N	**19.7543**	**15.6164**	**39.5712**	0.50917	0.96639	1.0308	**-1.6**	**6.1**	0.000110	Historic
Chahorra 1798 AD	TF338	**phonotephrite**	28R 334938E	3122468N	**19.7552**	**15.6164**	**39.5714**	0.50912	0.96633	1.0306	**-1.6**	**6.0**	0.000221	Historic
Garachico 1706 AD	TF341	**basanite**	28R 327138E	3138523N	**19.7197**	**15.6094**	**39.5184**	0.51019	0.96454	1.0267	**-1.9**	**5.0**	0.000313	Historic
Boca Cangrejo 1492 AD	TF330	**basanite**	28R 327526E	3129433N	**19.6783**	**15.6037**	**39.4842**	0.51167	0.96508	1.0287	**-2.0**	**6.6**	0.000527	Historic
Mt Reventada	TF332(c)	**basanite**	28R 329720E	3128762N	**19.7581**	**15.6132**	**39.5606**	0.50868	0.96503	1.0273	**-2.0**	**4.6**	0.0011	Carracedo et al., 2007
Mña. La Botija	TF377	**basanite**	28R 332226E	3127913N	**19.7587**	**15.6177**	**39.5753**	0.50907	0.96638	1.0307	**-1.5**	**6.0**	0.0036	Carracedo et al., 2006
Mña Abeque	TF380	**basanite**	28R 327616E	3130353N	**19.7527**	**15.6161**	**39.5693**	0.50921	0.96637	1.0307	**-1.6**	**6.1**	0.0090	Carracedo et al., 2007
La Caleta nodule	TF-L2-25G	**basaltic melt**	28R 358221E	3118883N	**19.8201**	**15.6229**	**39.6357**	0.50659	0.96648	1.0300	**-1.7**	**4.6**	0.221	Brown et al., 2003
La Caleta nodule	TF-L2-59G	**basaltic melt**	28R 358221E	3118883N	**19.7861**	**15.6173**	**39.5831**	0.50770	0.96460	1.0258	**-1.9**	**3.5**	0.221	Brown et al., 2003
Lava above Fasnia	TR010-10	**basanite**	28R 348255E	3128720N	**19.8394**	**15.6225**	**39.6422**	0.50563	0.96533	1.0269	**-1.9**	**2.9**	*0.281*	↑ Fasnia; ↓ Poris
Fasnia nodule	TF-L1-52G	**basaltic melt**	28R 357961E	3118928N	**19.8551**	**15.6247**	**39.6703**	0.50509	0.96655	1.0297	**-1.9**	**3.8**	0.289	Brown et al., 2003 & Edgar et al., 2007
Fasnia nodule	TF-L1-78Gii	**basaltic melt**	28R 357961E	3118928N	**19.8231**	**15.6221**	**39.6318**	0.50638	0.96584	1.0284	**-1.8**	**3.9**	0.289	
Fasnia nodule	TF-L1-79Gi	**basaltic melt**	28R 357961E	3118928N	**19.8433**	**15.6234**	**39.6543**	0.50553	0.96611	1.0288	**-1.9**	**3.7**	0.289	
scoria above La Tarta	TF19b	**basanite**	28R 353952E	3135097N	**19.8009**	**15.6182**	**39.6494**	0.50708	0.96956	1.0379	**-1.9**	**8.3**	*0.32*	↑ La Tarta pumice - no soil
Icod upper flow	TF339	**basanite**	28R 330998E	3138120N	**19.7349**	**15.6054**	**39.5800**	0.50905	0.96903	1.0377	**-2.5**	**9.3**	0.411	Carracedo et al., 2007
Icod upper flow	TF340	**basanite**	28R 330914E	3138169N	**19.7500**	**15.6070**	**39.5926**	0.50848	0.96884	1.0369	**-2.5**	**8.8**	0.411	Carracedo et al., 2007
sub-Fasnia lava, Magua	TF346	**phono tephrite**	28R 358196E	3118837N	**19.7491**	**15.6130**	**39.5997**	0.50909	0.96961	1.0388	**-1.9**	**9.6**	*0.44*	* Brown et al., 2003
sub-Fasnia lava, caldera	TR009-18	**tephrite**	28R 348202E	3128674N	**19.8398**	**15.6195**	**39.7103**	0.50533	0.97176	1.0427	**-2.2**	**9.7**	0.44	Ancochea et al, 1995
lava below La Tarta	TF19a	**tephrite**	28R 353911E	3135065N	**19.8211**	**15.6179**	**39.7105**	0.50607	0.97350	1.0473	**-2.2**	**12.0**	0.54	Ancochea et al, 1990
Mña. de Taco	TF342(a)	**basanite**	28R 320123E	3140412N	**19.7508**	**15.6174**	**39.6300**	0.50943	0.97234	1.0456	**-1.5**	**12.4**	0.706	Carracedo et al., 2007
sub-Arico lava, Magua	TF343	**basanite**	28R 358062E	3118447N	**19.7454**	**15.6114**	**39.5981**	0.50912	0.96980	1.0394	**-2.0**	**9.9**	*0.70*	Brown et al., 2003
average NE rift	*Deegan, 2012*	***basanite***	*28R 3550E*	*31350N*	***19.7776***	***15.6187***	***39.6632***	*0.51101*	*0.97303*	*1.0469*	***-1.6***	***12.5***	0.84	Carracedo et al., 2011
Playa de la Arena	TF333(a)	**basanite**	28R 319499E	3124744N	**19.7255**	**15.6097**	**39.6044**	0.50993	0.97225	1.0458	**-2.0**	**12.9**	0.901	Carracedo et al., 2007
North of Adeje	TF382	**basanite**	28R 330760E	3112630N	**19.7120**	**15.6037**	**39.5876**	0.51001	0.97190	1.0452	**-2.4**	**12.9**	*1.40*	Fuster et al., 1994
North of Adeje	TF383	**basanite**	28R 330977E	3112902N	**19.6644**	**15.6052**	**39.5460**	0.51250	0.97235	1.0472	**-1.7**	**14.5**	*1.40*	Fuster et al., 1994
Callao Salvaje lava	TF319	**basanite**	28R 323672E	3115991N	**19.7618**	**15.6085**	**39.5852**	0.50804	0.96704	1.0323	**-2.5**	**6.6**	*1.53*	Davilla-Harris et al 2013
sub-Adeje	TF 318	**basanite**	28R 323616E	3115996N	**19.7020**	**15.6027**	**39.5139**	0.51041	0.96574	1.0299	**-2.4**	**6.7**	*1.55*	Davilla-Harris, 2009
Morteros nodule	TR015-08	**basaltic melt**	28R 326957E	3110103N	**19.6196**	**15.5974**	**39.4270**	0.51397	0.96503	1.0295	**-2.0**	**8.0**	*1.75*	Davilla-Harris, 2009
Morteros nodule	TR027-12	**basaltic melt**	28R 327102E	3110408N	**19.6384**	**15.6037**	**39.4542**	0.51365	0.96592	1.0314	**-1.6**	**8.4**	*1.75*	Davilla-Harris, 2009
Gaviotas nodule	TR027-05	**basaltic melt**	28R 327037E	3110357N	**19.7943**	**15.6187**	**39.6000**	0.50744	0.96545	1.0278	**-1.8**	**4.2**	1.84	Huertas et al 2002
Gaviotas nodule	TF217	**basaltic melt**	28R 327006E	3110095N	**19.7592**	**15.6148**	**39.5601**	0.50877	0.96488	1.0270	**-1.8**	**4.4**	1.84	Huertas et al 2002
Gaviotas nodule	TF217	**amph+cpx+mte**	28R 327006E	3110095N	**19.7606**	**15.6152**	**39.5613**	0.50874	0.96486	1.0269	**-1.8**	**4.4**	1.84	Huertas et al 2002
Gaviotas nodule	TF217	**plagioclase**	28R 327006E	3110095N	**19.7458**	**15.6147**	**39.5431**	0.50942	0.96449	1.0262	**-1.7**	**4.3**	1.84	Huertas et al 2002
Teno														
Los Carrizales Alto	TF329	**phonolite**	28R 318095E	3134085N	**20.0187**	**15.6386**	**39.7171**	0.49867	0.95616	1.0024	**-2.2**	**-11.3**	5.9 - 6.1 Ma	Longpre et al., 2009
Roque del Conde														
Roque del Conde 1015m	TF368	**basanite**	28R 333151E	3109931N	**19.8704**	**15.6192**	**39.5862**	0.50383	0.95719	1.0066	**-2.6**	**-6.4**		
Roque del Conde 973m	TF369	**basanite**	28R 333165E	3109717N	**19.8172**	**15.6144**	**39.5347**	0.50593	0.95714	1.0070	**-2.5**	**-5.1**		
Roque del Conde 973m	TF369 (repeat)	**basanite**	28R 333165E	3109717N	**19.8216**	**15.6155**	**39.5383**	0.50582	0.95707	1.0068	**-2.4**	**-5.3**		
Roque del Conde 964m	TF370	**basanite**	28R 333154E	3109691N	**19.9845**	**15.6338**	**39.7024**	0.49982	0.95785	1.0069	**-2.3**	**-8.6**		
Roque del Conde 914m	TF371	**tephri-phonolite**	28R 333126E	3109603N	**19.9638**	**15.6301**	**39.6690**	0.50044	0.95657	1.0040	**-2.5**	**-9.4**		
Roque del Conde 871m	TF372	**phono-tephrite**	28R 333170E	3109522N	**19.9212**	**15.6269**	**39.6171**	0.50215	0.95552	1.0019	**-2.4**	**-9.5**		
Roque del Conde 815m	TF367	**phono-tephrite**	28R 333308E	3109328N	**19.9106**	**15.6250**	**39.6008**	0.50247	0.95494	1.0006	**-2.4**	**-9.8**		
Roque del Conde 810m	TF366	**phono-tephrite**	28R 333325E	3109330N	**19.9203**	**15.6254**	**39.5996**	0.50205	0.95395	0.9981	**-2.5**	**-11.1**	8.95 - 11.8 Ma	Thirlwall et al., 2000; Guillou et al., 2004
Roque del Conde 767m	TF365	**basanite**	28R 333442E	3109384N	**19.9643**	**15.6323**	**39.6556**	0.50063	0.95527	1.0009	**-2.3**	**-10.8**		
La Camella 366m	TF386	**phono-tephrite**	28R 335343E	3107603N	**19.9320**	**15.6324**	**39.5961**	0.50216	0.95258	0.9947	**-1.9**	**-12.9**		
Roque de Jama 563m	TF387	**tephri-phonolite**	28R 338861E	3107007N	**19.8840**	**15.6231**	**39.5636**	0.50356	0.95382	0.9982	**-2.3**	**-10.3**		
Roque de Jama 574m	TF388	**phonolite**	28R 338729E	3107751N	**19.8652**	**15.6280**	**39.5597**	0.50492	0.95516	1.0016	**-1.6**	**-8.4**		
Roque de Jama 593m	TF389	**phonolite**	28R 338812E	3108142N	**19.7841**	**15.6177**	**39.4631**	0.50784	0.95333	0.9980	**-1.8**	**-8.3**		
Roque de Jama 593m	TF389 (repeat)	**phonolite**	28R 338812E	3108142N	**19.7908**	**15.6187**	**39.4748**	0.50761	0.95383	0.9992	**-1.8**	**-7.9**		
under Caldera del Rey	TF348	**basanite**	28R 330851E	3107907N	**19.6441**	**15.5954**	**39.3131**	0.51256	0.95173	0.9955	**-2.5**	**-6.4**		
under Fanabe ignimbrite	TF 310(c)	**basanite**	28R 330408E	3110874N	**19.9570**	**15.6317**	**39.5951**	0.50092	0.95024	0.9888	**-2.3**	**-16.0**		

Acknowledgements:

Thanks to support from NERC Spitfire and Geological Society E. Mathews grants to RNT/EMRF. Andy Milton, Agnes Michalik, Ruth Davey, Lewis Bailey, Kim Dunn and Josh Brown are thanked for laboratory assistance. Discussions with Mike Norry, Richard Brown, Tiff Barry and Tim Elliott benefited this work. Thanks are also due to Maxim Ballmer and an anonymous reviewer for improving a previous version of this manuscript.

Author Contributions:

R.N.T. and E.M.R.F. analysed isotopes, P.D.H., M.B. and R.N.T. defined stratigraphy, R.N.T., E.M.R.F., T.M.G. completed fieldwork, R.N.T., T.M.G. and M.R.P. evaluated models. All authors contributed to writing the manuscript.

Authors:

Rex N. Taylor[1]	rex@soton.ac.uk
Pablo Davila-Harris[2,3]	pablo.davila@ipicyt.edu.mx
Michael Branney[3]	mjb26@leicester.ac.uk
E.M. Ruth Farley[1]	emruthfarley@gmail.com
Thomas M. Gernon[1]	Thomas.Gernon@soton.ac.uk
Martin R. Palmer[1]	mrp1@soton.ac.uk

Supplementary Information:

Mass fractionation correction of data originally measured by constant-f.

Figure S1 $^{206}Pb/^{204}Pb$ - $^{208}Pb/^{204}Pb$ *for Anaga samples – mass fractionation correction.*

Table S1 Compiled radiogenic isotope data for Canary Islands

Supplementary information

Mass fractionation correction of data originally measured by constant-f.

Where non-double spike data is used to provide locality and age-coverage, data is initially factorised to equate the quoted NBS SRM 981 values with the poly-spike average NBS 981 (Taylor et al., 2015). Pb isotope data not measured by double spike or MC-ICP-MS procedures (Tl-spike or sample-standard bracketing) assume a constant fractionation factor (*f*) for all samples based on the average value achieved for the repeated measurement of NBS SRM 981. This exposes results to an array of fractionation-related issues such as filament temperature and Pb-ionisation suppression due to the presence of residual matrix. In the case of some sample suites, such as Tenerife, there is a systematic relationship observed between $^{206}Pb/^{204}Pb$ and $^{207}Pb/^{204}Pb$ (Fig. 2) which can be tightly defined by regression. For the purposes of this correction it is assumed that this relationship holds for all samples from the island. Any difference between a constant-*f* datum and this line is then ascribed to deviation from the correct fractionation in its original measurement. In this way the measured sample, $^{206}Pb/^{204}Pb_s$ is projected along a mass fractionation line to intercept the $^{206}Pb/^{204}Pb$:$^{207}Pb/^{204}Pb$ regression line. General equations to calculate corrected $^{206\text{-}207\text{-}208}Pb/^{204}Pb_t$ are:

$$\frac{^{206}Pb}{^{204}Pb}_t = \left[\frac{^{207}Pb}{^{204}Pb}_s - \left(\frac{^{206}Pb}{^{204}Pb}_s * mf^{207}\right) - ct\right] \Big/ (ct - mf^{207})$$

$$\frac{^{207}Pb}{^{204}Pb}_t = mt * \frac{^{206}Pb}{^{204}Pb}_t + ct$$

$$\frac{^{208}Pb}{^{204}Pb}_t = \left(\frac{^{206}Pb}{^{204}Pb}_t * mf^{208}\right) + \frac{^{208}Pb}{^{204}Pb}_s - \left(\frac{^{206}Pb}{^{204}Pb}_s * mf^{208}\right)$$

Where

$\frac{^{20x}Pb}{^{204}Pb}_t$ $\frac{^{20x}Pb}{^{204}Pb}_s$ = ratios of fractionation corrected (*t*) and original measured (*s*) respectively

mf^{207}= gradient of $^{206}Pb/^{204}Pb$:$^{207}Pb/^{204}Pb$ fractionation line (1.1791 for linear fractionation)

mf^{208}= gradient of $^{206}Pb/^{204}Pb$:$^{208}Pb/^{204}Pb$ fractionation line (3.9836 for linear fractionation)

mt = gradient of $^{206}Pb/^{204}Pb$:$^{207}Pb/^{204}Pb$ "true" line (calculated as 0.09584 for Tenerife)

ct = intercept of $^{206}Pb/^{204}Pb$:$^{207}Pb/^{204}Pb$ "true" line (assumed as 13.7196 for Tenerife)

A natural limitation of the assumption that all samples have the same $^{206}Pb/^{204}Pb$-$^{207}Pb/^{204}Pb$ relationship is that some samples could have $^{207}Pb/^{204}Pb$ and $^{208}Pb/^{204}Pb$ increased by sediment contamination from either surficial (Saharan dust) or assimilated (crustal) material. In this case correction will result in marginally lower $^{206}Pb/^{204}Pb$. However, in the 121 samples measured in this study, only one was discordant to the $^{206}Pb/^{204}Pb$-$^{207}Pb/^{204}Pb$ regression. Corrected data from (Simonsen et al., 2000) is shown in Fig. S1.

Supplementary Fig. 1 *$^{206}Pb/^{204}Pb$ - $^{208}Pb/^{204}Pb$ for Anaga samples (Simonsen et al., 2000) re-corrected for mass fractionation assuming all Tenerife data follow the regression of double spike $^{206}Pb/^{204}Pb$ - $^{207}Pb/^{204}Pb$.*

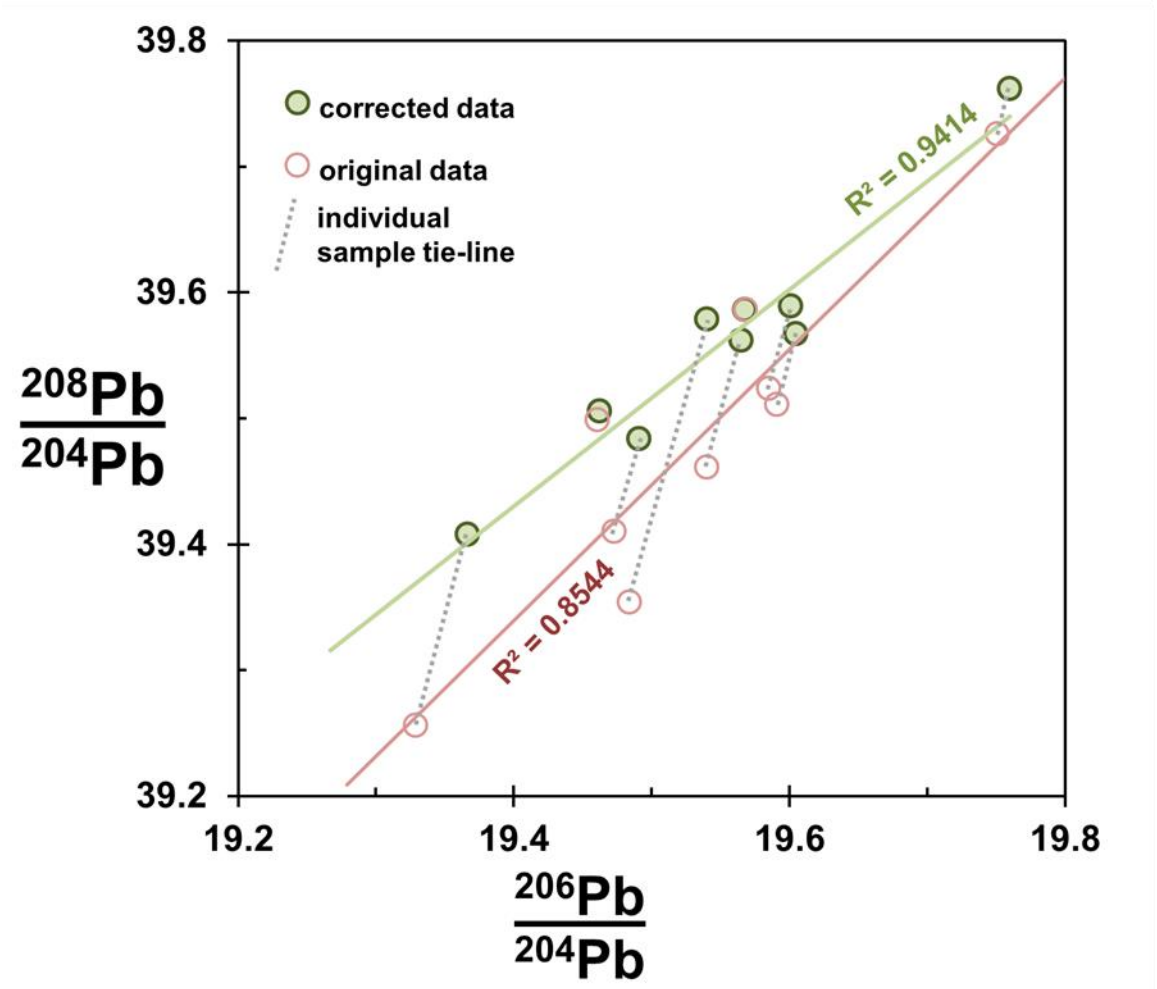

Table S1 Compiled radiogenic isotope data for Canary Islands

Island	unit	age range	$^{143}Nd/^{144}Nd$	$^{87}Sr/^{86}Sr$	$^{206}Pb/^{204}Pb$	$^{207}Pb/^{204}Pb$	$^{208}Pb/^{204}Pb$	208*/206*	208*t/206*t	Δ7/4	Δ8/4	n =	references
Tenerife	Bandas Del Sur cycle 3	0 - 0.5 Ma	0.51289	0.70314	19.782	15.617 #	39.600	0.9665	1.031	**-1.9**	**5.6**	38	**this study**
	Bandas Del Sur cycle 2	0.5 - 1.5 Ma	0.51288	0.70311	19.738	15.613 #	39.601	0.9708	1.042	**-1.8**	**11.1**	45	**this study, (Deegan et al., 2012)**
	Bandas Del Sur cycle 1	1.5 - 2.5 Ma	0.51286	0.70302	19.719	15.609 #	39.541	0.9667	1.032	**-2.0**	**7.3**	25	**this study**
	Anaga	3.9 - 4.9 Ma	0.51284	0.70317	19.537	15.575	39.497	0.9796	1.068	**-3.3**	**24.9**	8	**(Simonsen et al., 2000)**
	Anaga *(to Δ7/4 = 2.0)*	3.9 - 4.9 Ma			*19.550*	*15.590*	*39.549*	*0.9835*	*1.078*	***-2.0***	***28.6***	*8*	
	Teno	5.1 - 6.2 Ma	0.51291	0.70299	19.902	15.629	39.612	0.9568	1.005	**-2.0**	**-7.7**	14	**(Simonsen et al., 2000)**
	Roque de Conde	9 - 11.9 Ma	0.51289	0.70304	19.900	15.625	39.582	0.9541	0.999	**-2.3**	**-10.4**	17	**this study, (Gurenko et al., 2009)**
Lanzarote		0 - 0.1 Ma	0.51283	0.70317	19.186	15.551	38.971	0.9612	1.027	**-2.0**	**14.8**	31	**(Geldmacher et al., 2011; Sun, 1980; Thomas et al., 1999)**
La Palma	Cumbre Vieja	0 - 0.5 Ma	0.51290	0.70313	19.558	15.599	39.377	0.9660	1.033	**-1.2**	**10.4**	6	**(Abratis et al., 2002; Day et al., 2010; Geldmacher et al., 2011;**
	Taburiente/Bejenado	0.4 - 1.7 Ma	0.51291	0.70306	19.614	15.604	39.418	0.9647	1.029	**-1.3**	**7.8**	24	**Gurenko et al., 2006; Lundstrom et al., 2003; Praegel and Holm,**
	Basal Complex	3 - 4 Ma	0.51291	0.70308	19.842	15.629	39.604	0.9614	1.017	**-1.3**	**-1.3**	17	**2006; Sun, 1980)**
La Gomera		4.9 - 6 Ma	0.51289	0.70317	19.772	15.621	39.380	0.9465	0.981	**-1.3**	**-15.1**	1	**(Sun, 1980)**
		8 - 9.5 Ma	0.51291	0.70312	19.850	15.634	39.533	0.9541	0.999	**-0.9**	**-9.2**	9	**(Gurenko et al., 2006; Sun, 1980)**
Gran Canaria	Post Roque Nublo <1.3	0 - 1.3 Ma	0.51290	0.70318	19.504	15.606	39.403	0.9737	1.054	**0.0**	**19.6**	7	**(Aulinas et al., 2010)**
	Post Roque Nublo	1.7 - 3.0 Ma	0.51291	0.70315	19.399	15.583 #	39.318	0.9753	1.060	**-1.0**	**23.8**	10	**(Aulinas et al., 2010)**
	Roque Nublo	3.4 - 4.2 Ma	0.51286	0.70320	19.089 #	15.553 #	39.088	0.9828	1.088	**-0.7**	**38.3**	18	**(Hoernle et al., 1991)**
	El Tablero	4.2 - 4.5 Ma	0.51290	0.70310	19.418	15.577	39.190	0.9609	1.022	**-1.9**	**8.7**	5	**(Hoernle and Schmincke, 1993; Hoernle et al., 1991)**
	Fagtaga	11 - 12.9 Ma	0.51290	0.70311	19.835	15.605	39.595	0.9613	1.017	**-3.6**	**-1.2**	12	**(Cousens et al., 1993; Cousens et al., 1990)**
	Mogan	13.4 - 14.0 Ma	0.51291	0.70336	19.608	15.600	39.349	0.9585	1.013	**-1.6**	**1.5**	35	**(Cousens et al., 1993; Cousens et al., 1990)**
	Guigui/Hogarzales	14 - 15.0 Ma	0.51292	0.70335	19.547	15.605	39.291	0.9587	1.014	**-0.5**	**3.2**	20	**(Cousens et al., 1990; Gurenko et al., 2006; Gurenko et al.,**
	Submarine	15.8 - 17.4 Ma	0.51290	0.70319	19.802	15.617	39.589	0.9637	1.023	**-2.1**	**2.1**	3	**2010; Hoernle et al., 1991)**
Fuerteventura	Recent	0 - 1 Ma	0.51294	0.70310	19.224	15.563	39.005	0.9610	1.025	**-1.2**	**13.6**	10	**(Geldmacher et al., 2011; Hoernle and Tilton, 1991)**
	Miocene	13.5 - 16.5 Ma	0.51289	0.70321	19.576	15.591	39.374	0.9639	1.027	**-2.2**	**7.9**	8	**(Hoernle and Tilton, 1991; Sun, 1980)**
	Oligocene	25 -28 Ma			19.743	15.607	39.620	0.9721	1.045	**-2.5**	**12.4**	6	
El Hierro		0 - 1 Ma	0.51294	0.70299	19.380 #	15.583 #	39.058	0.9513	0.997	**-0.9**	**0.0**	16	**(Day et al., 2010; Geldmacher et al., 2011; Gurenko et al., 2009; Sun, 1980**

Abratis, M., Schmincke, H.U., Hansteen, T.H., 2002. Composition and evolution of submarine volcanic rocks from the central and western Canary Islands. International Journal of Earth Sciences 91, 562-582.
Aulinas, M., Gimeno, D., Fernandez-Turiel, J.L., Font, L., Perez-Torrado, F.J., Rodriguez-Gonzalez, A., Nowell, G.M., 2010. Small-scale mantle heterogeneity on the source of the Gran Canaria (Canary Islands) Pliocene–Quaternary magmas. Lithos 119, 377-392.
Cousens, B.L., Spera, F.J., Dobson, P.F., 1993. Posteruptive alteration of silicic ignimbrites and lavas, Gran Canaria, Canary Islands - strontium, neodymium, lead, and oxygen isotopic evidence. Geochimica Et Cosmochimica Acta 57, 631-640.
Cousens, B.L., Spera, F.J., Tilton, G.R., 1990. Isotopic patterns in silicic ignimbrites and lava flows of the Mogan and lower Fataga Formations, Gran Canaria, Canary Islands: temporal changes in mantle source composition. Earth and Planetary Science Letters 96, 319-335.
Day, J.M.D., Pearson, D.G., Macpherson, C.G., Lowry, D., Carracedo, J.C., 2010. Evidence for distinct proportions of subducted oceanic crust and lithosphere in HIMU-type mantle beneath El Hierro and La Palma, Canary Islands. Geochimica Et Cosmochimica Acta 74, 6565-6589.
Deegan, F.M., Troll, V.R., Barker, A.K., Harris, C., Chadwick, J.P., Carracedo, J.C., Delcamp, A., 2012. Crustal versus source processes recorded in dykes from the Northeast volcanic rift zone of Tenerife, Canary Islands. Chemical Geology 334, 324-344.
Geldmacher, J., Hoernle, K., Hanan, B.B., Blichert-Toft, J., Hauff, F., Gill, J.B., Schmincke, H.U., 2011. Hafnium isotopic variations in East Atlantic intraplate volcanism. Contributions to Mineralogy and Petrology 162, 21-36.
Gurenko, A.A., Hoernle, K.A., Hauff, F., Schmincke, H.U., Han, D., Miura, Y.N., Kaneoka, I., 2006. Major, trace element and Nd-Sr-Pb-O-He-Ar isotope signatures of shield stage lavas from the central and western Canary Islands: Insights into mantle and crustal processes. Chemical Geology 233, 75-112.
Gurenko, A.A., Hoernle, K.A., Sobolev, A.V., Hauff, F., Schmincke, H.-U., 2010. Source components of the Gran Canaria (Canary Islands) shield stage magmas: evidence from olivine composition and Sr-Nd-Pb isotopes. Contributions to Mineralogy and Petrology 159, 689-702.
Gurenko, A.A., Sobolev, A.V., Hoernle, K.A., Hauff, F., Schmincke, H.-U., 2009. Enriched, HIMU-type peridotite and depleted recycled pyroxenite in the Canary plume: A mixed-up mantle. Earth and Planetary Science Letters 277, 514-524.
Hoernle, K., Schmincke, H.U., 1993. The role of partial melting in the 15 Ma geochemical evolution of Gran Canaria - a blob model for the Canary hotspot. Journal of Petrology 34, 599-626.
Hoernle, K., Tilton, G., Schmincke, H.U., 1991. Sr-Nd-Pb isotopic evolution of Gran-Canaria - evidence for shallow enriched mantle beneath the Canary Islands. Earth and Planetary Science Letters 106, 44-63.
Hoernle, K., Tilton, G.R., 1991. Sr-Nd-Pb isotope data for Fuerteventura (Canary Islands) basal complex and subaerial volcanics: application to magma genesis and evolution. Schweizerische Mineralogische und Petrographische Mitteilungen 71, 5-21.
Lundstrom, C.C., Hoernle, K., Gill, J., 2003. U-series disequilibria in volcanic rocks from the Canary Islands: Plume versus lithospheric melting. Geochimica Et Cosmochimica Acta 67, 4153-4177.
Praegel, N.O., Holm, P.M., 2006. Lithospheric contributions to high-MgO basanites from the Cumbre Vieja Volcano, La Palma, Canary Islands and evidence for temporal variation in plume influence. Journal of Volcanology and Geothermal Research 149, 213-239.
Simonsen, S.L., Neumann, E.R., Seim, K., 2000. Sr-Nd-Pb isotope and trace-element geochemistry evidence for a young HIMU source and assimilation at Tenerife (Canary Island). Journal of Volcanology and Geothermal Research 103, 299-312.
Sun, S.S., 1980. Lead isotopic study of young volcanic-rocks from mid-ocean ridges, ocean islands and island arcs. Philosophical Transactions of the Royal Society a-Mathematical Physical and Engineering Sciences 297, 409-445.
Taylor, R.N., Ishizuka, O., Michalik, A., Milton, J.A., Croudace, I.W., 2015. Evaluating the precision of Pb isotope measurement by mass spectrometry. Journal of Analytical Atomic Spectrometry 30, 198-213.

Thomas, L.E., Hawkesworth, C.J., Van Calsteren, P., Turner, S.P., Rogers, N.W., 1999. Melt generation beneath ocean islands: A U-Th-Ra isotope study from Lanzarote in the Canary Islands. Geochimica Et Cosmochimica Acta 63, 4081-4099.

references

this study
this study, (Deegan et al., 2012)
this study
(Simonsen et al., 2000)

(Simonsen et al., 2000)
this study, (Gurenko et al., 2009)

(Geldmacher et al., 2011; Sun, 1980; Thomas et al., 1999)

(Abratis et al., 2002; Day et al., 2010; Geldmacher et al., 2011; Gurenko et al., 2006; Lundstrom et al., 2003; Praegel and Holm, 2006; Sun, 1980)

(Sun, 1980)
(Gurenko et al., 2006; Sun, 1980)

(Aulinas et al., 2010)
(Aulinas et al., 2010)
(Hoernle et al., 1991)
(Hoernle and Schmincke, 1993; Hoernle et al., 1991)
(Cousens et al., 1993; Cousens et al., 1990)
(Cousens et al., 1993; Cousens et al., 1990)
(Cousens et al., 1990; Gurenko et al., 2006; Gurenko et al., 2010; Hoernle et al., 1991)
(Gurenko et al., 2010)

(Geldmacher et al., 2011; Hoernle and Tilton, 1991)
(Hoernle and Tilton, 1991; Sun, 1980)

(Day et al., 2010; Geldmacher et al., 2011; Gurenko et al., 2009; Sun, 1980)